REACTION SYNTHESIS OF HfB_2 IN A VARIETY METALLIC ENVIRONMENTS

By

C. Patrick Dykema

Thesis submitted to the faculty of the
Virginia Polytechnic Institute and State University
in partial fulfillment of the requirements for the degree of

Master of Science

in

Materials Science and Engineering
Stephen L. Kampe, Chair
Alexander O. Aning
Gary R. Pickrell

July 30, 2009
Blacksburg, VA

Keywords: Reaction Synthesis, SHS, hafnium dibroide,

Reaction Synthesis of HfB_2 in a Variety of Metallic Environments

C. Patrick Dykema

Abstract

This project investigated the reactive formation of hafnium diboride (HfB_2) in a variety of metallic environments, including blends with Bi, Cu, Ni, and Sb. HfB_2 has garnered interest for a variety of applications due to its hardness, stability at elevated temperatures, as well as electrical and thermal conductivity. Experimental testing included differential scanning calorimetry (DSC) to reveal reaction initiation temperatures and enthalpies of reaction; and optical pyrometry to measure maximum reaction temperatures.

Overall, DSC results indicated melting preceded reaction initiation; suggesting that the reaction initiation temperature for a certain blend occurred soon after melt formation, and could be broadly approximated by examination of binary phase diagrams. However, compositions containing bismuth ignited almost 200 ºC above the expected melting temperature.

The maximum temperature measurement did not appear to correlate with reaction enthalpies as might be expected. This lack of correlation may be a result of an inability to capture the true maximum temperature due to the measurement frequency of the pyrometer, the disparity of heating rates between the two experimental methods, and/or to the influence of intermediate reactions on the temperature increase.

Table of Contents

List of Figures

List of Tables

Overview

1.1 Summary

This investigation explores the formation of HfB_2 from its elemental components in a variety of metallic environments including alloys comprised of bismuth, copper, nickel, antimony and tin. The formation of HfB_2 is highly energetic. Its reaction from elemental constituents results in relatively large exothermic reaction enthalpies and high reaction temperatures. Despite the reaction's high thermodynamic driving force, its initiation typically requires an externally-applied thermal stimulus to overcome a variety of kinetic constraints inherent to powder-based processing methodologies. Conducting the reaction in the presence of a metallic solvent has been demonstrated to be an effective way to reduce and engineer the ignition temperature of the reaction, but also serves to dilute the per-mass energy output of the formulation.

This project attempts to survey the reactivity of various hafnium-boron-X (Hf-B-X) blends, where X represents a ductile metallic dilutent incorporated within the pre-reacted formulation. Additional constraints guiding the selection of the specific metallic diluents (i.e., X) examined in this study are provided in subsequent sections. Specifically, experimental data was obtained in an attempt to establish for each diluted formulation:

1.) whether the HfB_2 reaction could be initiated and sustained; and if so,

2.) an estimate of the ignition temperature,

3.) the peak temperature attained during the reaction, and

4.) an estimate of the overall heat of reaction.

The above information will serve as preliminary screening data towards assessing the viability of the metallic-containing formulations for their use as structural reactive materials.

1.2 The Project

The project investigates reactive mixtures of elemental metal powders that spontaneously react to form a blend of more stable compounds, one of which will be hafnium diboride (HfB_2). The purpose for this research is the development of reactive processing science and more specifically, the general application area known as structural energetic materials. Energetic materials are defined as materials that store chemical energy in the form of enthalpy; the enthalpy can be released by facilitating a reaction to a more stable chemical phase state. Structural energetic powder blends are additionally characterized by an ability to achieve full densification in the pre-reacted, compacted state such that useful mechanical or structural properties are attained concurrent with the storage of enthalpy. Thus, effective structural reactive materials will feature high enthalpic energy output, tunable or controllable ignition characteristics, and strengths that enable the pre-reacted blend to serve in a load-bearing capacity. For certain applications of energetic materials, formulations that additionally result in high theoretical material density (TMD) values are also of interest.

For this project, certain HfB_2-based structural energetic material formulations have been preliminarily identified by compositions that include hafnium, boron, and a ductile metal as pre-reaction components. As mentioned above, the reaction of hafnium and boron to form hafnium diboride results in a relatively large enthalpy change released in the form of heat. The ductile metal acts as a binder that serves to facilitate compaction thus enabling the attainment of

structural-capable mechanical properties. Boron exhibits a low ductility and high volume fraction for the HfB_2 stoichiometry; bcc-hafnium is only moderately ductile and occupies a small volume fraction due to its high density. As a result, the metallic diluents with high ductility serve as binding agents.

Additional characteristics sought in the ductile metallic binder in this study include a propensity to reactively-form hafnium-based intermetallic(s) and a low melting temperature. Intermetallic compound formation is exothermic and its formation from elemental reactants can contribute to, rather than strictly dilute, the total heat output of the formulation. Low melting temperatures are useful in their facilitation of reaction initiation. An illustrative and well-known example of a structural reactive formulation is represented by blends based on the Hf-B-Al system. In this regard, both HfB_2 and Hf-based aluminide intermetallics will form as products of reactive processing. Initiation of the reaction has been found to be concurrent with the melting of aluminum (1), rather than the much higher temperatures that would be otherwise required in the absence of aluminum within the formulation.

1.3 Properties of Diborides

The Group IV diborides, namely TiB_2, ZrB_2, and HfB_2 are sometimes referred to as ultra-high temperature ceramics due to their stability with rising temperatures. There is a wide range of use for these materials in environments with elevated operating temperatures, and also as particles within metal matrix composites. Other applications exploit various material properties such as high thermal and electrical conductivity, as well as thermal shock and oxidation resistance at

elevated temperatures (2). A summary of relevant properties is detailed below in Table I along with comparative information for ZrO_2, a common high temperature ceramic oxide.

Table I:
Properties of group IV diborides and ZrO_2 (2,3)

	TiB_2	ZrB_2	HfB_2	ZrO_2
T_m(°C)[a]	2920-3050	3040	3100-3250	2550-2700
Thermal Conductivity (W/mK) [b]	25-65	20-60	70-80	1.7-2
Electrical Resistivity (μohm/cm) [b]	10-50	10-20	20-50	3×10^{15}-10^{16}
Approximate Cost for Metal only (Ti/Zr/Hf) (US$/kg)	40 99% pure	20-30	120-140 97% pure	18-27 Cost for ZrO_2

Above information compiled from (2,3)
a: Temperatures are approximate due to difficulty measuring in this range
b: Values vary depending on the source of information (also temperature dependent)

1.4 Applications of Diborides

Applications of group IV diborides include a variety of thermal shielding from furnace linings and plasma arc electrodes (4), to leading edges of aircraft for re-entry from space. (5) TiB_2 and ZrB_2 have been investigated most extensively. One reason for this is that titanium and zirconium are more abundant and less expensive than hafnium based materials, and therefore viable for more applications. Titanium alloys are used for applications requiring strong, lightweight materials such as for the aerospace industry. Zirconium is used extensively by the chemical industry for its exceptional durability under acidic and alkali environments as well as by the nuclear industry. Hafnium based composites have limited applicability due to high material costs; although they are used for nuclear applications such as fuel control rods that exploit their high absorbance of thermal neutrons (6).

The nature of the diboride bond is very stable, thus the large negative enthalpy of formation. The reaction between hafnium and boron appears to behave in a similar manner to the commonly known thermite reaction. However, there is no exchange of oxygen; rather there is only a formation of HfB_2 from pure elements that release the energy. The formation energy and the associated stability of the diboride make reaction synthesis an attractive route to strengthen bulk composites through in-situ formation of precipitates.

Beyond exothermic formation energies, group IV diborides are especially known for hardness, which is exploited through use in abrasives and reinforcement precipitates. Example abrasive applications include cutting, grinding, or drilling. Example applications of a reinforcement phase include: strengthening of bulk material for structural components, coatings for high temperature shielding, and components for demanding environments such as welding electrodes (4).

1.5 Energetic Materials

A wide range of energetic materials are commonly used, from fuels to explosives. Each is selected for specific characteristics such as: energy content, density, price, availability, or stability. Many 'high energy,' or explosive, materials in use are a variety of carbon and nitrogen based compounds; upon combustion the formation of compounds such as: CO_2, H_2O, CO, and NO_x generate much of the energy released. However, gases generated at the reaction front serve to limit peak reaction temperatures through convective cooling. In contrast, the formation of diborides is typically comprised of solid state reactions that, nominally, do not form gases as a consequence of the reaction. Instead, elemental reactants combine to form products in the solid

state. Although convective cooling still occurs, the effects are reduced by the elimination of gases produced at the reaction front. Gasless combustion reactions tend to exhibit practical reaction temperatures closer to the theoretical adiabatic temperature of reaction.

A comparison of the energies of formation and adiabatic temperatures for the Group IV diborides is shown below in Table II; values are provided for a reaction initiating at 298 K. The adiabatic temperature is defined as the maximum theoretical temperature attained during the reaction, and is computed assuming that all change in enthalpy for a reactive system serves to elevate the sample's temperature with no environmental energy loss.

Table II:
Energetic Characteristics of Monolithic Diborides (7)

	TiB_2	ZrB_2	HfB_2
Heat of Formation $\Delta_f H_{298K}$ (kJ/mol)	278	301	322
$\Delta T_{ad\ 298K}$ (°C)	2890	3010	3220

From comparing enthalpies of reaction and adiabatic temperatures, it is apparent that moving down the fourth column of the periodic table shows a steady rise in energy of reaction and the associated maximum reaction temperature. With HfB_2 about ten percent above TiB_2 with respect to these formation energies, we look to the hafnium based reactions as a way to maximize energy output while favoring high theoretical material density (TMD) in the pre-reacted compacts.

Background Theory

2.1 Reaction Synthesis or SHS (Self-propagating High-temperature Synthesis)

In the 1960's Merzhanov, Borovinskaya, and Shkiro discovered the highly exothermic nature of mixtures of titanium and boron while investigating combustion of solids. Initially coining the term solid flame, or solid combustion; it is now often referred to in the literature as combustion or reaction synthesis.

Two general modes of reaction have been observed, namely, equilibrium and non-equilibrium with distinctly different means of reaction. Equilibrium combustion indicates that the combustion products are formed concurrently with the reaction wave; the mechanism of reaction is diffusional. Reactions happen at component interfaces and can produce products with layered structures of multiple phases. Non-equilibrium reactions form meta-stable phases in the reaction wave that subsequently transform to the final products behind the combustion wave. Meta-stable phases of the non-equilibrium type may include: melt, amorphous structure, and oversaturated liquid or solid solutions. Non-equilibrium reactions are characterized by a wide reaction zone and very rapid SHS propagatiom (8).

SHS is a newer term to essentially represent solid combustion. It is generally characterized as reactions that, once initiated, carry through to completion driven by the energy released as the reaction progresses, requiring no further energy input. A widely known example is the thermite reaction; a process by which two ingredients, a metal and a metal oxide are mixed and ignited (9). As one oxide breaks down, a new more stable oxide forms; resulting in an overall exothermic reaction. The energy released from forming the more stable oxide drives the

decomposition of the initial oxide, effectually fueling the reaction. A common thermite reaction between aluminum and iron (III) oxide is used for welding railroad track, cutting steel sections, and in pyrotechnics. It is detailed in equation 1 below:

$$2Al + Fe_2O_3 \rightarrow Al_2O_3 + 2Fe + heat \qquad (1)$$

Combustion, or reaction synthesis, also describes a SHS process. However, these terms typically indicate that the reaction's principal purpose lies in generating the products. Reaction synthesis is advantageous in forming intermetallics for ease, effectiveness, and cost efficiency (9). Both pure intermetallics and composite materials may be formed. Reaction synthesis of composites is attractive due to the strong bonding exhibited by reinforcement particles with the host matrix during in-situ formation (10). In fact, the mechanical properties of combustion synthesized composites have been observed to have increased strength, modulus, and creep resistance (10).

Other techniques relying on mixing the intermetallic matrix composite (IMC) components after formation tend to exhibit poor bonding at the particle/matrix interface. Combustion synthesis overcomes the low wetting of various metals on the synthesized ceramic, tends to be more cost efficient, and often yields a better product (4). Reaction synthesized materials can be made in near-net shape to minimize additional processing and machining. Compounds with high melting temperatures can be fabricated through reaction synthesis due to the reaction temperatures achieved.

2.2 Specific Reactions Involving HfB_2

HfB_2 can be formed through an exothermic SHS process; however there is no exchange of oxygen in the manner illustrated in equation. 1. Instead, the diboride may be formed from its pure components according to the reaction shown below in equation 2.

$$Hf + 2B \rightarrow HfB_2 + heat \qquad (2)$$

In this case, the indicated heat evolved represents the heat of reaction for monolithic HfB_2. With a metallic diluent (e.g., Al) and additional Hf incorporated into the formulation appropriate to the stoichiometry of a stable intermetallic (e.g., HfAl), the reaction will be

$$(x-1)\cdot Al + x\cdot Hf + 2\cdot B \rightarrow (x-1)\cdot HfAl + HfB_2 + heat \qquad (3)$$

The evolved heat represents the heat of reaction for the indicated product mixture. Prior investigation into the formation of HfB_2-Al composites through reaction synthesis found the reaction initiation temperature to be concurrent with the melting of aluminum (1). The study by Yi et al on the synthesis of HfB_2-Al composites observed two distinct combustion zones moving with the reaction; one reaction zone appeared more luminous. After quenching during the reaction, samples observed through SEM reveal Al_3Hf at the reaction front. However, when the reaction is allowed to progress to completion, HfB_2 and aluminum were the dominant products with only residual traces of Al_3Hf (1). These results suggest that upon melting, the reaction forms an intermetallic compound that subsequently undergoes a displacement reaction resulting in HfB_2.

Once a liquid forms, it can wet the solid particles and spread. At the liquid/solid interface the reaction ensues, releasing energy to drive the reaction forward. Thus, at the reaction front a liquid phase moves through the material as combustion propagates. For multi-component systems investigated, a number of intermetallics are believed to form in the liquid region as intermediary compounds that subsequently break down to generate the diborides.

2.3 Incipient or Eutectic Melts

Melting point depression, or the shift in stability of liquid phase to lower temperatures, is usually seen in multi-component systems. Typical behavior near the edges of a binary phase diagram is for the melting point of either pure substance to be depressed by the presence of the other. This phenomenon is observed and often exploited during powder-based processing. Here, contact points among the various components of powder blends will, with minimal diffusion required, establish compositional gradients that lead to melting point depressions.

At elevated temperatures diffusion occurs quickly and localized solid solutions form which in turn melt and spread over the powder interface before the pure components melt. This localized, interfacial melting phenomenon is known as incipient melting, illustrated in Figure 1. It is the mechanism that drives the process known as liquid phase sintering, and relevant to the initiation of SHS reactions in the manner of equation 3, which commence upon melt formation.

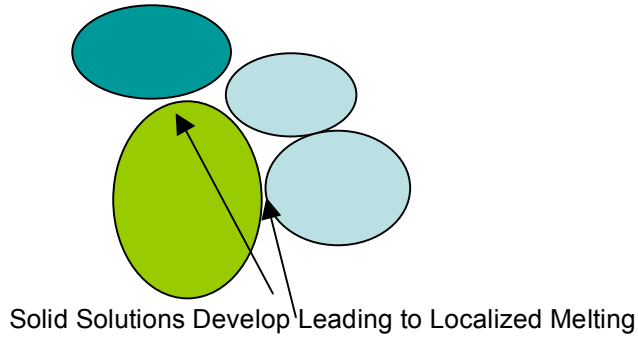

Figure 1: Illustration of incipient melting at particle interfaces.

Incipient melting is further encouraged by the fact that impurities and defects preferentially concentrate at grain boundaries and surface interfaces during crystallization on account of the favorable reduction in energy (11). These regions facilitate the development of solid solutions due to the presence of impurities and a disruption of bonding periodicity.

2.4 Liquid Phase Sintering

The term sintering refers to a process where powdered blends are consolidated through subjugation to a thermal cycle. Compacted powders generally sinter at temperatures above one-half their absolute melting temperature, allowing for material processing well below the melting temperature of bulk material (12). The large surface area present in consolidated powders serves as a driving force for bond formation with neighboring particles, thus reducing surface area. Used for firing clay based bricks several thousand years ago (12); sintering is a common step to aid powder consolidation for powder processing of all types of materials.

Liquid phase sintering simply indicates that a liquid phase coexists with the solid as part of the process. For powder blends with more than one component, a liquid phase typically develops

due to melting point depression, and especially within the range of a eutectic composition and temperature. Powder blends with a mixture of elemental components form solid solutions at particle interfaces. With rising temperatures a eutectic composition and blend are attained through diffusion, thus forming liquid regions. Due to capillary action, localized pressure drives spreading of the liquid phase through cavities between solid particles (12). A chemical reaction assists wetting between the solid and liquid phases, which further facilitates spreading of the liquid (12).

2.5 Role of Diffusion

Atomic diffusion is used to describe atomic movements that result in short and long range compositional changes; quantitatively, it represents a flux describing the quantity and rate at which atoms move. Several factors are responsible for the activation of diffusion; the most easily recognized is concentration gradient. Additionally, temperature and stress gradients as well as surface effects encourage atomic motion to achieve an equilibrium state (13). The diffusion coefficient itself is temperature dependent, with increasing temperature, diffusion rates rise (13).

For this project, diffusion in both solid and liquid phases are relevant and important. Solid state diffusion enables localized component mixing which may allow for incipient melting (12); the presence of either incipient liquid or long range melting enhances diffusion and component mixing; which may lead to the initiation of the intended reactions.

Measurements of Interest / Analytical Methods

3.1 Differential Scanning Calorimetry (DSC)

A calorimeter is a device used to measure and monitor energy in the form of heat; a DSC compares the difference in heat input required to increase the temperature of a sample relative to a known reference. The difference in signals of the sample relative to the reference reveals specific heat and changes of energetic state indicative of phase changes. The DSC will thus be capable of capturing, as a function of increasing temperature, the chronology and heat flux associated with any melting events, and/or the enthalpy changes associated with a reaction. The integrated area under the heat flux curve over the non-linear region associated with the reaction provides an estimate of the enthalpy of formation. An inflection change in the heat flux output typically signals the initiation of a reaction.

3.2 Infrared Pyrometer

Pyrometry indirectly measures an object's temperature by sensing incident radiation with a photo-electric detector whose electrons are easily excited to higher energy levels. Higher temperatures increase radiation intensity; this radiation excites electrons in sensor material, resulting in a voltage. The voltage output is calibrated with known systems to represent the measured reactions temperature. An infrared sensor is used because peak radiation intensities generated up to 4000 K lie in the near-infrared region (NIR) see Figure 2 for a graphical explanation (14). The pyrometer used for our experiments senses radiation of wavelengths close

to 1μm, this correlates closely with the maximal spectral radiance a blackbody emits in the temperature range of interest: 2000-3000 K.

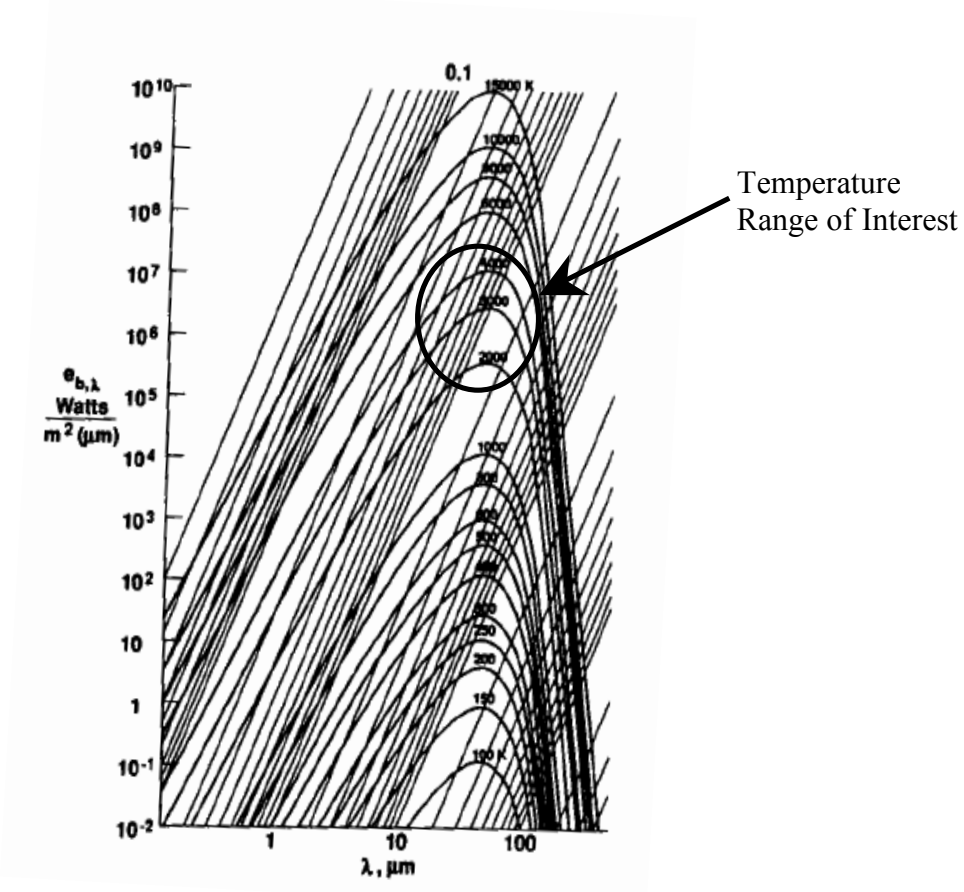

Figure 2: Planckian curves of spectral radiant power for various blackbody temperatures
Used with (kind) permission of the von Karmen Institute for Fluid Dynamics, 2011

All objects above the theoretical zero Kelvin energy reference are known to radiate energy due to inherent atomic vibrations. With increasing temperatures, radiation intensity or flux increases as motion escalates. An object's total emissive power over all wavelengths is proportional to temperature to the fourth power (T^4) through a relation known as the Stephen-Boltzmann equation. A blackbody exhibits complete absorption of insipid radiation or maximal emission of radiation for a given temperature, indicative of an emissivity of one or unity. Experimentally encountered materials do not radiate the maximal amount of thermal radiation and are known as

gray bodies. They demonstrate an emissivity below one, which is proportional to the amount of electromagnetic radiation produced at a given temperature.

The emissivity of a material is difficult to characterize accurately. It changes with temperature, wavelength, and surface characteristics such as angle of incidence, roughness, and degree of oxidation. Beyond discrepancies arising from sample emissivity, the infrared radiation that is emitted must travel through the atmosphere to reach a sensor device. Atmospheric contamination such as water vapor or fine particulates of smoke and dust may absorb radiation at some wavelengths, decreasing apparent intensity. The main absorptions due to water vapor, however, lie outside of our pyrometers range; near wavelengths of 2.5 and 6 μm (15).

The most robust system, therefore, operates in a strictly regulated, known atmosphere with numerous reference points of the sample temperature measured through pyrometry that is confirmed with a thin-wire thermocouple. These calibrations allow for a changing value of emissivity to account for variations in emitted radiation wavelength and sample temperature. This is a time intensive process that has not been well characterized for the vast majority of materials; therefore two-color pyrometers which use an intensity ratio are often used instead.

The ratio method relies on an assumption that changing emissivity and atmospheric absorption will affect both wavelengths equally, thereby negating these effects through a ratio. A further implication of these assumptions is that emissivity is independent of wavelength, or in other words, a target's emissivity is constant over changing wavelengths, which can only be valid in narrow wavelength regions. If these assumptions are not met, a two-color technique has the

potential to produce far greater errors in measurement than a monochromatic method because a faulty emissivity is factored in twice.

A two-color pyrometer made by LumaSense Technologies Inc. (M770S) was used throughout experimentation to measure maximum temperatures of reaction. Many details of the instrument are not released to consumers, however, the manufacturer did concede to using two wavelengths close to each other and near 1 μm in length. These are the so-called two colors; the closer they are in wavelength the more likely it is that emissivity is equivalent for both wavelengths. Instrument consistency is limited by the capability to produce materials with narrow absorption ranges that are distinct; or more simply put: two colors which are close, but not the same. The sensor material operates based on the well known photo-voltaic effect which allows for a quick response time on the order of 10 milliseconds.

An interesting table concerning error in pyrometry, distributed by the manufacturers of our pyrometer, is shown below in Figure 3 (16). It is important to note that these errors would be expected for an ideal blackbody system simply limited by calibration accuracy. In applications, numerous other factors introduce additional error, for example: changing emissivity with temperature, variations in wavelength intensities with changing emissivity, phase changes during the reaction sequence affect on emissivity, and impedance of sight path. As such, a significantly wider uncertainty range is expected for real systems; uncertainties of +- 100-300 °C are easily feasible, however difficult to quantify.

U(single color, 2-color), etc. = Uncertainty (k=2) of the single color measurement, 2-color, etc. at the time of calibration aimed at the blackbody.

Temp C°	U (single color)	U (2-color) °C	U (2-color) °F	Equivalent e-ratio or "slope"
800	0.5	11.2	20.2	0.987
1100	0.7	15.8	28.4	0.989
1500	0.9	20.1	36.2	0.991
1900	1.1	24.6	44.3	0.993
2700	3.0	66.4	119.5	0.990

Figure 3: Uncertainty of pyrometer measuring blackbody temperatures denoted by U *(k=2 indicates confidence interval of approximately 95 %)* (16)
Used with (kind) permission of LumaSense Technologies, 2011

3.3 Powder X-Ray Diffraction

X-ray diffraction (XRD) operates based on the fundamental principle that waves interact with a periodic lattice to produce interference patterns. Polycrystalline materials may be evaluated through powder XRD based on the assumption that a finely ground sample will consist of randomly dispersed and oriented crystallites.

X-rays are filtered to produce a narrow, distinct beam that is targeted at a powdered sample. The incident angle of the beam is slowly changed to yield a wave interference pattern. Depending on the crystal structure, certain incident angles will constructively interfere to produce peaks on the interference pattern.

Resulting data from an x-ray diffractometer shows the intensity of a diffracted peak as a function of incident angle of the x-ray beam. This series of peaks can be compared with patterns of known crystalline phases to confirm phases that are present.

Procedure

4.1 Material Selection

Due to the correlation between reactive material ignition and the onset of reactant melting, a range of metals were selected based on their melting temperature as candidate diluents in the reactive formulation. In addition, because of the eventual need for these materials to be densified into structural form, ductility is also influential for its potential role as a binder in a powder densification process and has likewise been surveyed and included as a selection criterion. As mentioned previously, density of the compact is also of interest for structural energetic material applications.

Specific formulations were prepared based on a 40 volume percentage (post-reacted) loading of HfB_2, with the balance composition established by an assumed known intermetallic composition within the hafnium-metal binary equilibrium system. These formulations do not indicate actual products present in the post-reacted product.

Table III summarizes the nominal compositions assumed for purposes of the formulation, and the mass percentages utilized for each formulation. A brief summary of properties relevant to the selection criteria (hardness, ductility, melting temperature, and inherent density) of the elemental reactants that comprise and support the formulations listed in Table III is provided in Table IV.

In two instances (NiBi and NiSb intermetallics), density of the targeted intermetallic composition was not available; for these, formulations were developed based on a 40 mass percent diboride / 60 mass percent intermetallic product. The comparison of columns on the far left and right of Table III indicates that the volume and mass percents are quantitatively similar in value.

Table III:
Component formulation information as a function of an assumed intermetallic / HfB_2 product mixture.

Nominal (Target) post-reacted Composition	Pre-reacted Component	Vol %	Pre-reacted Mass %	Mass % HfB2	Mass % Inter-metallic
$Cu_{51}Hf_{14}$ - 40 v% HfB_2	Copper	35.9	33.4	40.9	59.1
	Hafnium	45.8	62.2		
	Boron	18.2	4.4		
Ni_5Hf - 40 v% HfB_2	Nickel	39.0	36.5	41.3	58.7
	Hafnium	42.8	59.0		
	Boron	18.2	4.5		
Ni_7Hf_2 -40 v% HfB_2	Nickel	35.0	32.1	40.0	60.0
	Hafnium	47.1	63.6		
	Boron	17.9	4.3		
NiHf - 40 v% HfB_2	Nickel	17.9	15.3	38.0	62.0
	Hafnium	63.9	80.6		
	Boron	18.2	4.1		
Sb_2Hf - 40 v% HfB_2	Antimony	42.2	32.7	43.3	56.7
	Hafnium	40.7	62.6		
	Boron	17.1	4.7		
Sn_2Hf - 40 v% HfB_2	Tin	40.7	33.4	41.5	58.5
	Hafnium	42.2	62.1		
	Boron	17.1	4.5		
$HfBi_2$ - 40 v% HfB_2	Bismuth	43.4	43.4	38.1	61.9
	Hafnium	39.3	52.5		
	Boron	17.3	4.1		
Cu_2Sb - 40 v% HfB_2	Copper	24.7	27.2	46.7	53.3
	Antimony	32.1	26.1		
	Hafnium	25.8	41.7		
	Boron	17.5	5.0		
NiBi - 40 w% HfB_2	Nickel	13.6	13.2	40.0	60.0
	Bismuth	44.1	46.8		
	Hafnium	25.1	35.7		
	Boron	17.1	4.3		
NiSb - 40 w% HfB_2	Nickel	17.0	19.5	40.0	60.0
	Antimony	47.5	40.5		
	Hafnium	21.1	35.7		
	Boron	14.3	4.3		

Table IV:
Selected material properties of components used in formulations during the present study (3).
Note: Values were not measured from our raw materials.

	Hardness (Vickers)	Ductility (% elongation)	Melting Temperature (°C)	Density gm/cm3
Hafnium	155-195	20-45	2150	13.1
Boron(fiber)	800	0.5	2300	2.3
Antimony	5-10	5-15	630	6.7
Bismuth	5-10	20-30	270	9.8
Copper	50-100	25-50	1083	8.9
Nickel	100-200	15-60	1453	8.9
Tin	3-5	55-75	232	7.3

Table V details some of the specifics including the source and purity of the raw materials used throughout experimentation.

Table V:
Details relevant to reactants for powders used in this study.

Material	**Source**	**Purity**	**Details**
Hafnium	AEE	99.5 %	-325 mesh
Boron	AEE	95.0-97.0 %	1 µm APS
Antimony	Sigma-Aldrich	99.5 %	-100 mesh
Bismuth	Cerac	99 %	-325 mesh
Copper	AEE	99.9 %	-325 mesh
Nickel	AEE	99.5 %	-325 mesh
Tin	AEE	99.5 %	-325 mesh

4.2 Powder Processing

The constituent powders were transferred into an argon-environmental glove box where they were weighed in the proportions shown in Table III. Elemental ingredients of each formulation were placed in a glass vial which was in turn placed in a LDPE nalgene bottle. A contained iron oxide absorbate packet designed to eliminate any possible oxygen contamination was placed within the plastic bottle. The bottles were then placed on a rolling mill to homogenize the mixture, running at approximately 40 rotations per minute for 24 hours.

Once blended, the mixture was transferred in air to a hardened steel die, 12.7 mm (0.5 in) in diameter, and pressed with a uniaxial load applied through a manuallly-operated hydraulic Carver press. A water soluble rubber based lubricant was generously applied to the interior of the die and worked between moving parts. The die requires lubrication due to the abrasiveness of boron which constitutes a large volume fraction of the blends. Samples were pressed to 57.8 kN(13,000 lbs_f), as read on the pressure gauge, resulting in a uniaxial pressure of approximately 456 MPa (66,200 psi). During compaction, the pressure was noted to drop off with time due to powder rearrangement; therefore once the samples were compacted at the target pressure, a minute was allowed to elapse for relaxation of the load, at which point the die was re-pressurized to 57.8 kN. The resulting compacts were used to section samples for DSC approximately (0.8 mm, 0.031 in thickness), and for the pyrometry studies (6.4 mm, 0.25 in) discussed later.

4.3 Reaction Initiation Temperatures

Ignition temperature for each formulation was determined using the differential scanning calorimeter (DSC). The pressing of the material into compacts represents the samples' first exposure to an unregulated atmospheric environment containing significant amounts of oxygen. Thus, samples were evaluated immediately after pressing to minimize time of atmospheric exposure. A piece from the compact was broken off and weighed using a precision digital balance then loaded into a new alumina DSC crucible with lid. Another new crucible with no sample was prepared to act as a baseline; both crucibles were placed onto the sample carrier of the internal DSC chamber. High purity argon was added as a shielding gas at an approximate flow rate of 25 ml/min and was maintained throughout the heating cycle. Once the gas has been flowing for several minutes to flush the chamber, the gravimetric balance stabilizes and the sequence was initiated. The specific temperature profile included a constant heating rate of 40 ºC/min up to 1400 ºC with samples ranging between 30-100 mg in mass.

Heating cycle times for each trial generally required several hours including cooling. Samples were run successively one after the next over the course of about twelve hours to reduce accumulated oxidation effects. Prior to each DSC temperature program, the unit was calibrated using two empty crucibles as per manufacturer-described protocol.

Interpretation of DSC data hinges on the second differential of the energy output curve; an abrupt deviation in the rate of rate of change indicates that the reaction has initiated. Figure 4 represents a typical DSC curve indicating example boundaries for data interpretation based on the second differential. The DSC software automatically represents the 'onset' temperature by a

change in inflection; therefore, the practical ignition temperature is often a bit lower than the reported value depending on the peak width. For cases with more than one exothermic peak, the ignition temperature corresponds with the largest peak; as seen upon examination of DSC graphs for the Cu_2Sb (Figure 11) and Ni_5Hf (Figure 6) systems, which show multiple clear exothermic peaks.

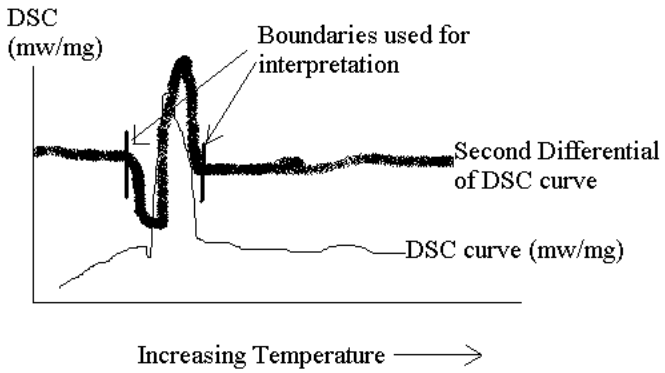

Figure 4: Example curve of DSC results and interpretation.

4.4 Reaction Enthalpies

Reaction energies were determined from the same DSC curves obtained as described above in section 4.3. Magnitudes were determined by measuring the area below a DSC curve; the unit's software computes this value through integration. The boundaries for this area were selected by the operator to coincide with changes in the second differential as seen in Figure 4.

Interpretation of DSC curves for both ignition and reaction enthalpy relies on human interpretation of the results. Many compositions produced clear results with easily defined second differential boundaries. However, some compositions showed unclear reaction; for which, difficulties of interpretation resulted in an omission of data in the results tables.

4.5 Maximum Reaction Temperatures

For peak temperature measurements, the infrared pyrometer requires a warm-up time of about thirty minutes once plugged in. Larger compacts were reacted on a silica refractory platform within a box furnace set to 1000 ºC; several other pieces of refractory brick placed around the reaction platform shielded the furnace interior. The pyrometer, placed on a table about six feet away from the box furnace, was protected by a polycarbonate shield to stop debris from striking the lens. A sight on the pyrometer was centered and focused on the planned place of reaction; at which point the pellet was carefully placed at the focused spot with a pair of tongs and safety equipment to protect from the heat. For these experiments, no heating rate is measured; empirically the pellets were observed to go from ambient temperature to reaction in less than a minute, which varied depending on composition. Effective heating rates were on the order of 1000 ºC per minute, significantly higher than those of the DSC (40 ºC/min).

The pyrometer has a published response time of 7.5 ms to detect about 60% of incident radiation; the effective response time for complete detection is longer. Data collection yielded eight temperature measurements per second; in some cases, the first temperature measured was also the maximum temperature. For these compositions, higher temperatures may have been experienced prior to pyrometric measurement.

4.6 Powder X-Ray Diffraction

Reacted compacts used for pyrometric studies were analyzed with x-ray diffraction (XRD) towards the identification of crystalline phases following reaction synthesis. Samples were prepared as described in Section 4.2; and subsequently reacted in a box furnace under atmospheric conditions as described in Section 4.5. A SPEX mill was used to reduce the post-reaction sample to a powder suitable for XRD analysis. SPEX mills operate by vigorously shaking a container with the sample and several milling media, in this case, three tungsten-carbide balls. Thirty minutes of milling resulted in a fine powder that could easily be packed into a sample holder for XRD analysis. Major diffraction peaks for crystals which contain any combination of the constituents in a blend, including atmospheric elements, fell between a 2Θ angle of 25° and 50°. Therefore, all samples were scanned over a 25° range with a step size of .03°.

Upon completion of a scan, the data was transferred to a computer that plots intensity of peaks as a function of incident angle. To determine present phases, known intensity patterns of possible phases were superimposed over the measured intensity peaks for comparison.

Results and Discussion

5.1 Reaction Initiation Temperatures

Table VI shows the ignition temperature data for each nominal composition studied. Shown are the raw results for up to four trials each, the average, and a standard deviation for the data. The entry, "similar," indicates that the DSC trace exhibited a comparable distinct reaction ignition, but the subsequent reaction was poorly defined and therefore difficult to interpret, yielding no enthalpy value.

Table VI:
Experimental data of ignition temperatures from the DSC

Nominal Composition		Ignition Temperature (°C)						
40 v%	60 v %	1	2	3	4	Average	Standard Deviation σ	Coefficient of Variance V[a]
HfB_2	$Cu_{51}Hf_{14}$	Similar	1022.9	1014		1018		0.0062
HfB_2	Ni_5Hf	1097.8	1087.8	1088.2		1091	5.7	0.0052
HfB_2	Ni_7Hf_2	1085.3	1086	1028.7	1082.6	1070	28	0.026
HfB_2	NiHf	1072.4	1073	1071.4	1073.5	1073	0.90	0.00084
HfB_2	Sb_2Hf	Similar	594.7	588	587.6	590	4.0	0.0068
HfB_2	Sn_2Hf							
HfB_2	Bi_2Hf	488	497	485.3	477	487	8.2	0.017
HfB_2	Cu_2Sb	Similar	685.4	685.4	Similar	685		
HfB_2	NiBi	Similar	475	Similar		470		
HfB_2	NiSb	624.5	622.9	621.4	621.6	623	1.4	0.0023
HfB_2	NiSb (NiReduced)	616.1	613.9	612.6		614	1.8	0.0029

Standard deviations for two or less data points are not included
a: Coefficient of Variance is simply the standard deviation divided by the mean

Ignition temperatures, when measurable, show reasonable consistency and reproducibility. With two exceptions, the standard deviation is within 1% of the mean. Exceptions include the Ni_7Hf_2 and Bi_2Hf compositions where the standard deviation was within 3% of the mean.

The cells are left blank for the Sn_2Hf composition because the DSC yielded no interpretable information other than the endothermic reaction associated with tin melting around 230 ºC. Upon observation of the DSC crucible after testing, a metallic film was seen completely separated above the constituent blend; indicating no reaction had occurred. Analysis for this composition is discussed in further detail in the 'tin' paragraph of section 5.5.

The specific formulations don't necessarily indicate that these phases form in the indicated percentages, mentioned in section 4.1. All compositions allot for the formation of HfB_2 in an environment of various matrix metals. The practical ignition temperature is a little below recorded values from DSC curves due to the automatic measuring of onset temperature by a change in inflection.

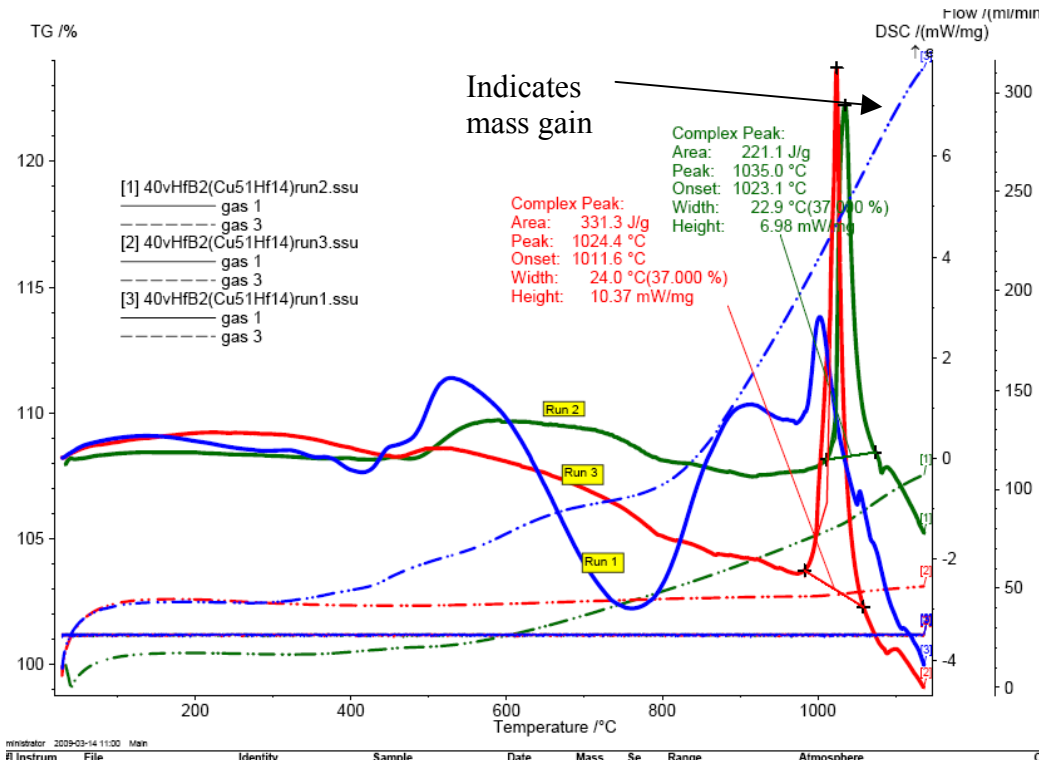

Figure 5: DSC curve for the nominal $Cu_{51}Hf_{14}$ composition.

DSC data for the $Cu_{51}Hf_{14}$ composition, presented in Figure 5, shows a large mass gain for the first trial (blue trace) and unclear reactions; however, the second and third trials (green and red traces, respectively) show a clear exothermic reaction beginning around 1000 ºC representative of ignition. The Cu-Hf phase diagram shows several phases with liquid stable from 970 ºC and up, however, the DSC curve does not indicate a melting endotherm leading into ignition. It is possible that the ignition endotherm is too small to register considering the phase diagram, which suggests a liquid can be stable near 970 ºC. Or, perhaps, a solid intermediate phase formed during heat-up undergoes a displacement reaction to form hafnium diboride upon ignition. An interesting observation is that the lowest melting temperature in the Cu-B system occurs around 1013 ºC; which, incidentally, is very close to the observed ignition temperature. For this formulation, a ternary phase diagram for Hf-Cu-B may yield more insight about ignition.

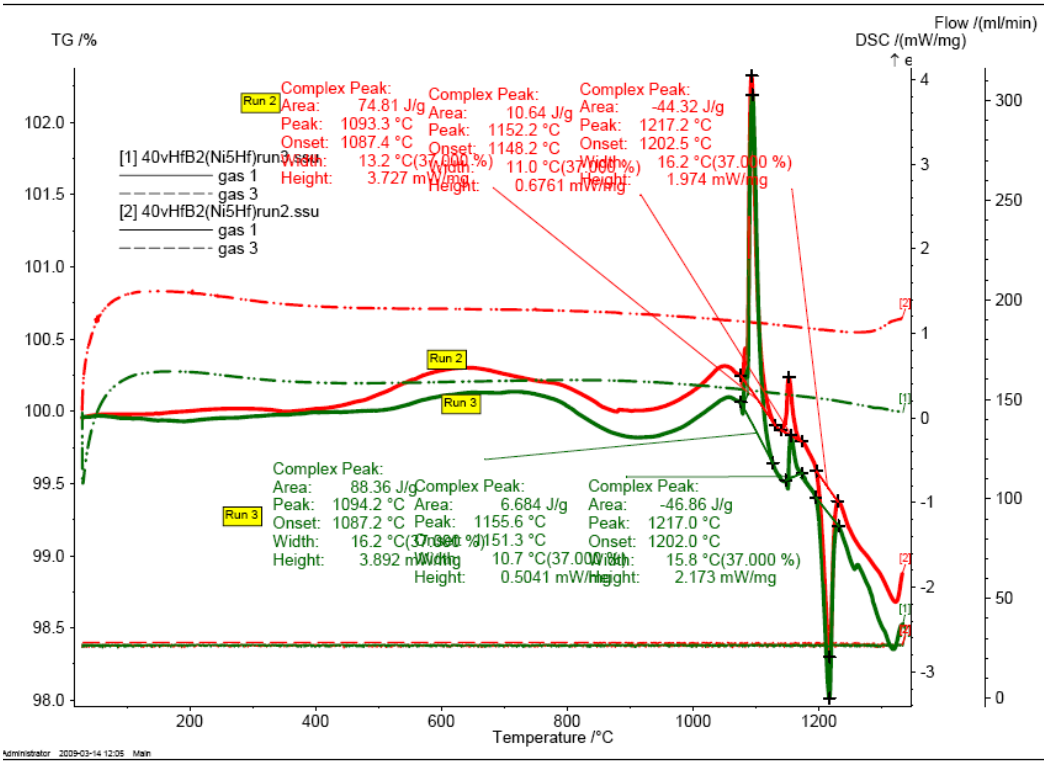

Figure 6: DSC curve for the nominal Ni_5Hf composition.

DSC curves for the Ni_5Hf composition, as seen in Figure 6, are consistent for the second (red) and third (green) trials. The first trial is not included because there is no clear reaction sequence. The curves show an endothermic melting leading directly into the major exothermic reaction just below 1100 ºC. A second, smaller endo/exotherm pair is observed around 1150 ºC, and a final melting endotherm begins near 1200 ºC. The Ni-B phase diagram contains the lowest temperature at which liquid is stabile in this system, near 1018 ºC; although close to the measured ignition temperature, the difference suggests diffusion limiting the compositions available at particle interfaces.

The second set of reactions at 1150 ºC may indicate the melting and decomposition of Ni-B or Ni-Hf intermediates formed during the initial reactions. The final endotherm is substantial, on the order of 45 J/g near 1200 ºC; possibly due to the melting of a Ni-Hf intermetallic phase several of which melt around 1190ºC as shown on the Ni-Hf phase diagram.

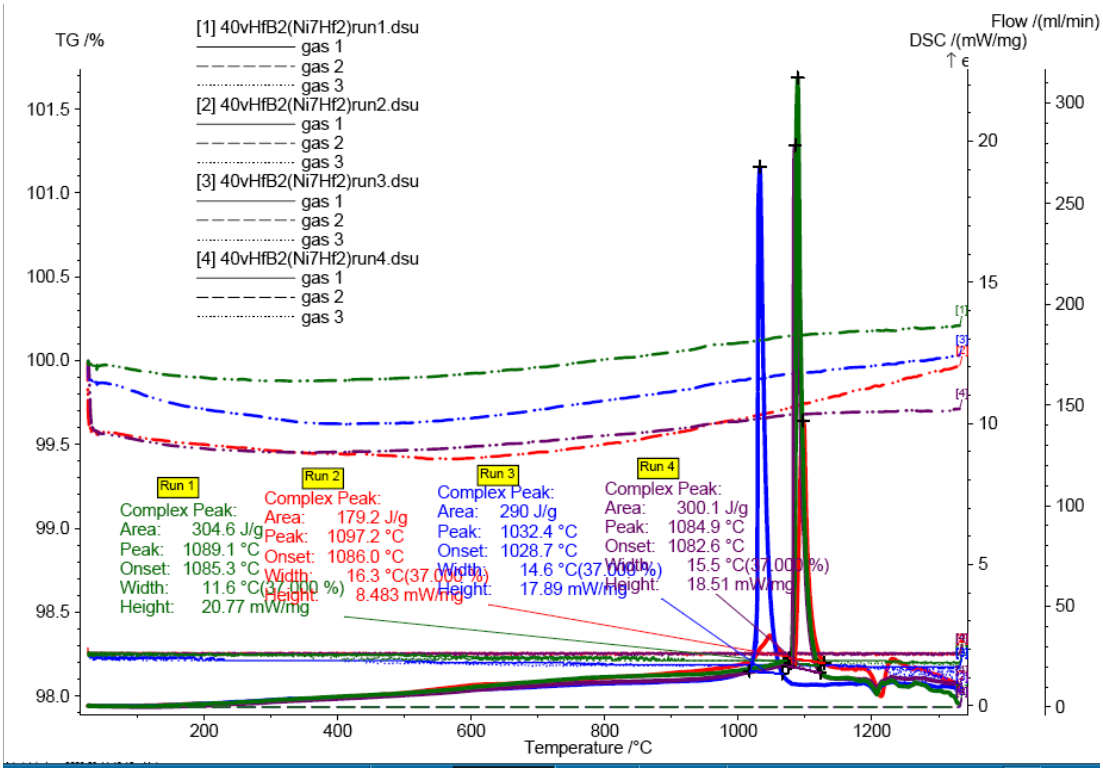

Figure 7: DSC curve for the nominal Ni_7Hf_2 composition.

The Ni_7Hf_2 formulation yielded clear DSC curves, shown above in Figure 7; however, the third trial ignited approximately 50 ºC before the others, just above 1000 ºC. This ignition temperature matches well with the lowest temperature stable liquid in the Ni-B system of 1018 ºC. The second trial also began to indicate an early reaction, but then delayed the main exotherm to coincide with the first and fourth trials beginning around 1080 ºC. This is evidence that the

formation of liquid for these compositions may be easily disturbed; possible explanations include: intermediate compounds formed while heating or fluctuations in packing inherent through the compaction process.

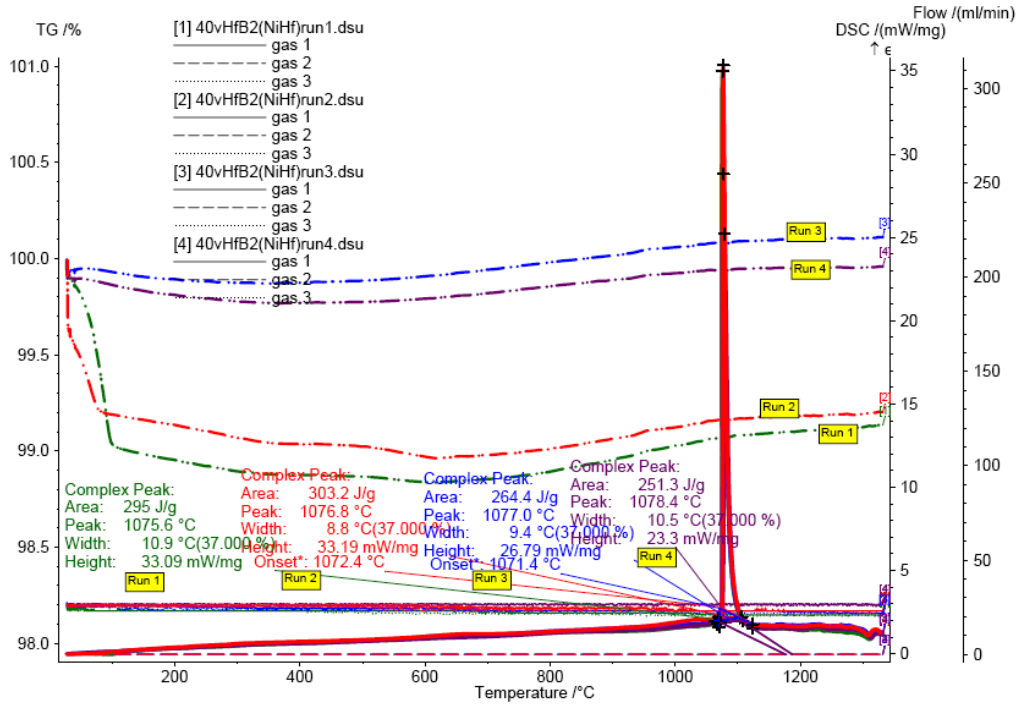

Figure 8: DSC curve for the nominal NiHf composition.

DSC curves for the NiHf composition (Figure 8) displayed uniformity between trials with a small endotherm leading into the single exothermic reaction around 1080 ºC. This endothermic reaction is too small to see in Figure 8, but is revealed upon close examination of an enlargement. Ignition most likely coincides with the melting of a Ni-B intermediate as discussed in the previous two paragraphs on Ni-Hf systems. The Ni-B phase diagram indicates stable liquid as low as 1018 ºC.

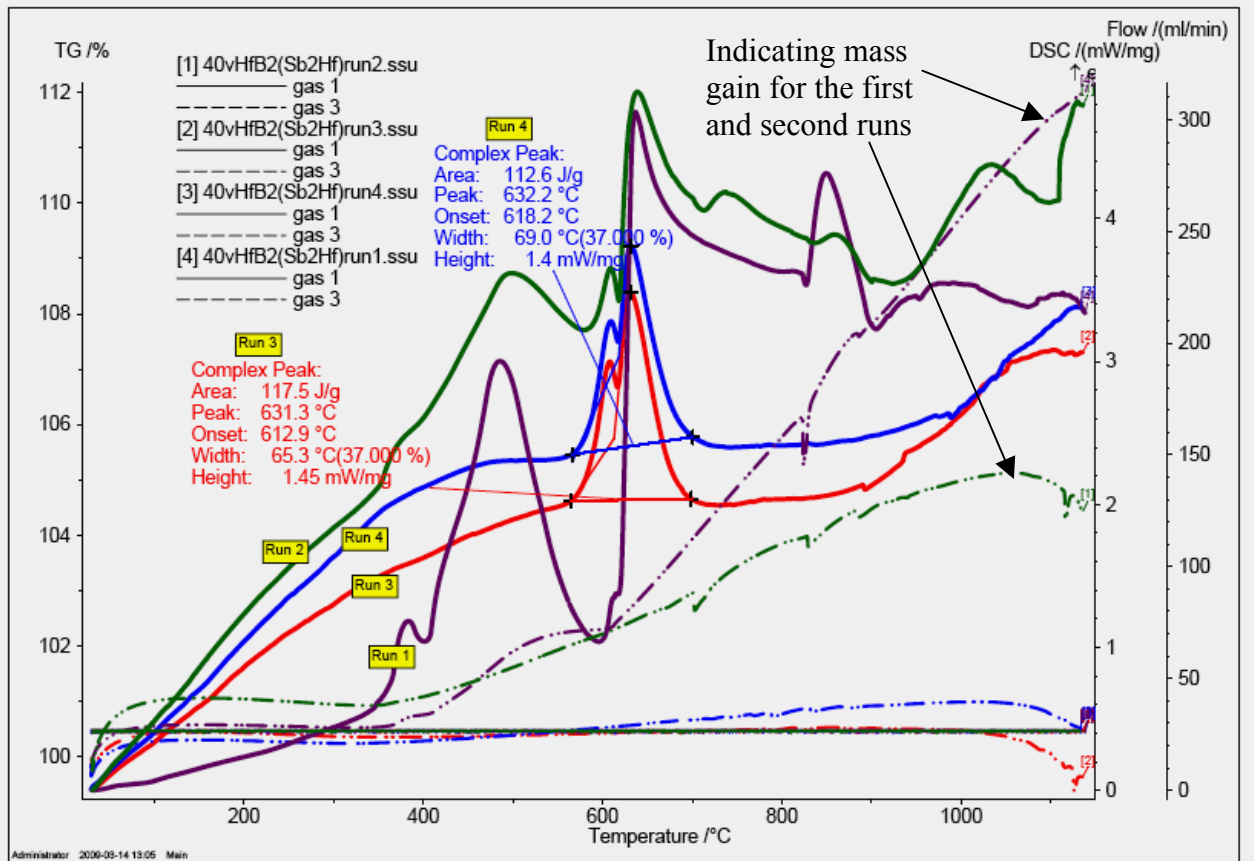

Figure 9: DSC curve for the nominal Sb_2Hf composition.

For the Sb_2Hf composition shown in Figure 9, the first two trials are noted to exhibit irregularities and mass gain; however, the third and fourth trials yield consistent data. Although a Sb-Hf phase diagram is not available, the Sb-Ti phase diagram indicates the lowest melting point is near that of pure antimony, 630 ºC. The ignition temperature for this composition occurs around 590 ºC with no melting indicated; which is shortly thereafter interrupted by a melting endotherm just over 600 ºC. This interruption suggests that intermetallic formation in the solid state may precede and actually drive first melting for this system.

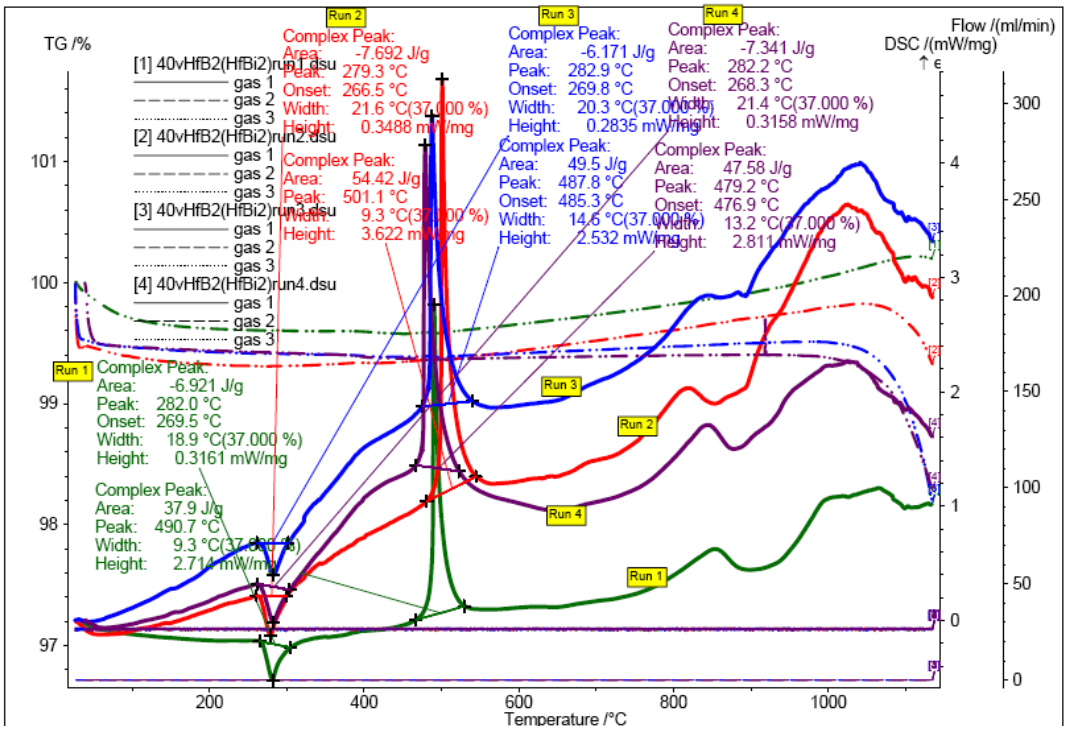

Figure 10: DSC curve for the nominal Bi_2Hf composition.

The Bi_2Hf composition yielded very consistent DSC graphs (Figure 10). The results show a melting endotherm just below 270 ºC for all trials, but the exothermic reaction is delayed until near 480 ºC. The endotherm corresponds well with the melting temperature of pure bismuth; although the Bi-Hf phase diagram available only covers the bismuth rich region, the Bi-Zr diagram also indicates 271 ºC as the lowest temperature at which liquid is stable. The exothermic peak reveals ignition for this composition around 470 ºC. This temperature appears to be the lowest temperature at which reactions ignite, also seen in the NiBi compact (Figure 12). This temperature limit may coincide with the melting of boron oxide, which occurs around 450 ºC. If this reasoning is accurate, the oxide layer covering boron restricts motion enough to stop reactions from ensuing and must melt to initiate a reaction.

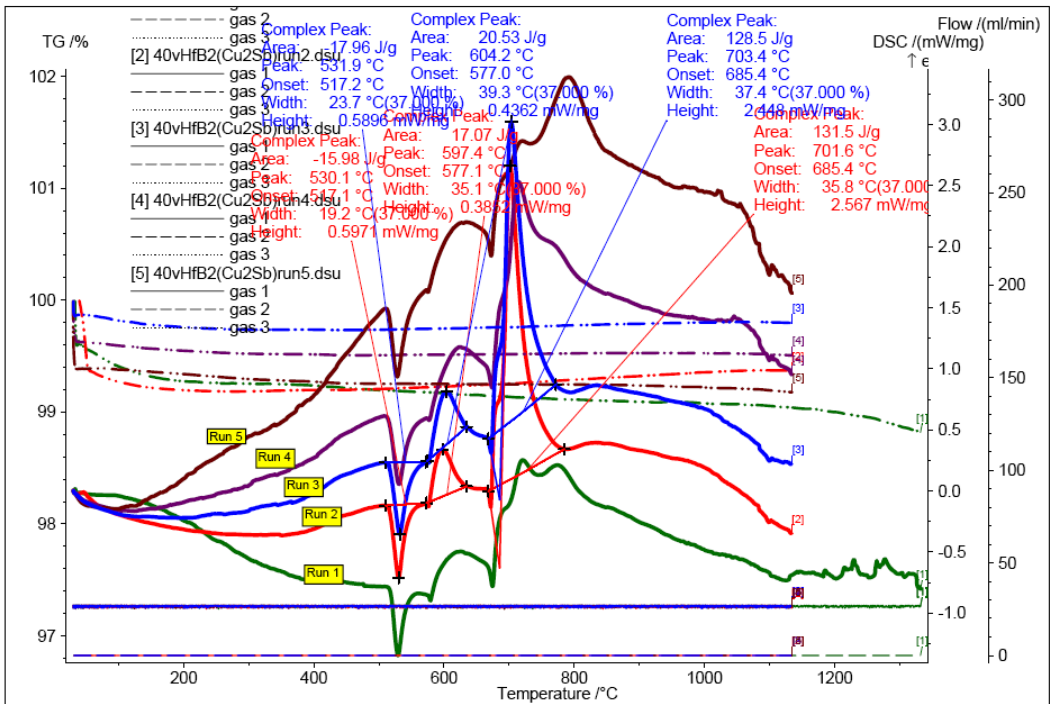

Figure 11: DSC curve for the nominal Cu_2Sb composition.
(A DSC chart with only trials 2 and 3 is available in Appendix A).

The Cu_2Sb compact DSC curves seen in Figure 11 exhibit progressive evolution from the first to the fifth run, indicating this composition is especially influenced by time effects. Although some trials did not yield distinct enthalpies, the ignition peaks are clearly consistent. The curves display distinct melting between 520 ºC and 570ºC followed by a small exothermic peak on the order of 20 J/g near 580ºC. This corresponds with the lowest temperature of a stable liquid phase at 526 ºC on the Cu-Sb phase diagram; indicating the incipient melting of antimony followed by an exothermic release associated with forming an intermetallic. Apparently the products from this initial reaction melt, producing a second smaller endotherm around 680 ºC, which leads directly into the main exothermic event. Ignition recorded in Table VI above corresponds to the second, larger exothermic reaction.

The Cu-Sb phase diagram consists of phases with broad composition ranges without strict proportions; for this system, the most stable intermetallic phase with elevating temperatures contains 20-30 atomic percent antimony denoted by β. The liquidus of this phase has a peak value of 683 ºC, which is very interesting because it corresponds quite closely to the melting and ignition observed near 685 ºC. Perhaps the β phase is formed during the first reaction and subsequently deteriorates to fuel diboride formation.

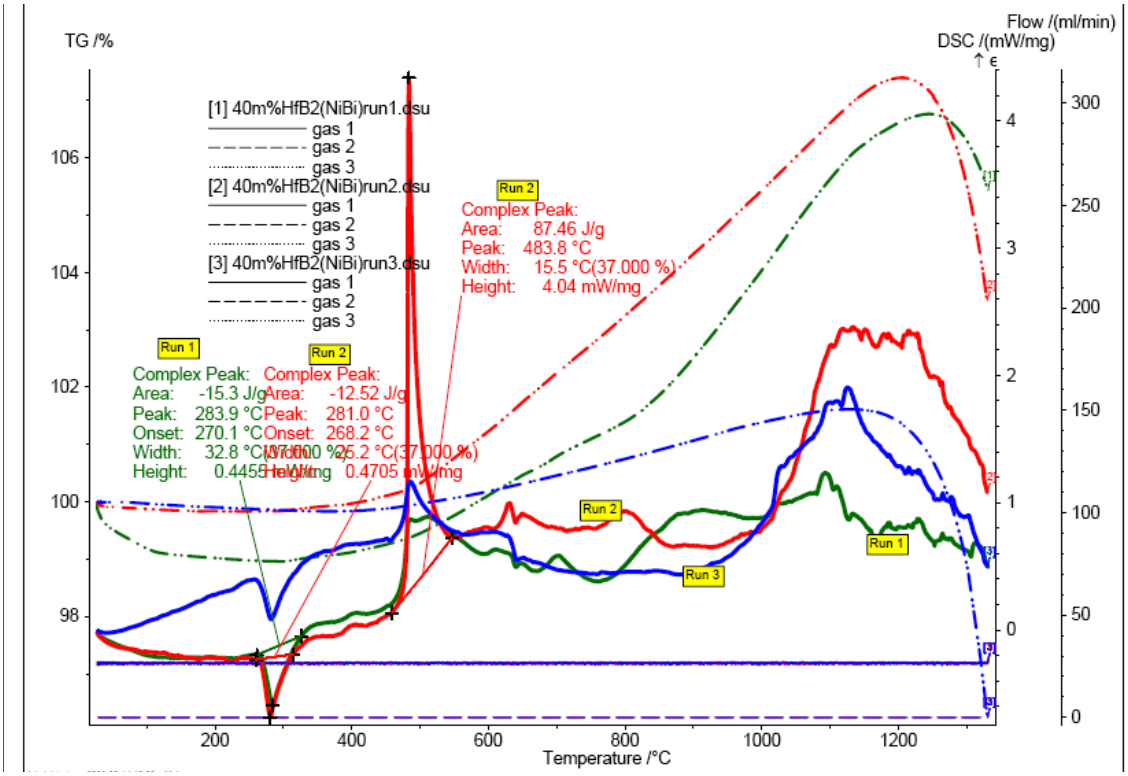

Figure 12: DSC curve for the nominal NiBi composition.

The DSC curves for the NiBi formulation (Figure 12) show some deviations in shape, although all trials indicate a melting endotherm around 270 ºC followed by an exothermic reaction.

Ignition, marked at the inflection of the exothermic curve around 480 ºC, is comparable to the ignition temperature of the Bi_2Hf composition (Figure 10). The curves show a mass gain of about 6 % for the first two samples; the changing curve shapes between trials indicates this composition may be sensitive to time effects; such as the oxidation of the compact before testing. Ignition is marked at the inflection of the exothermic curve, around 480 ºC, and is comparable to the ignition temperature of the Bi_2Hf composition (Figure 10). Observation of the Ni-Bi phase diagram indicates an intermetallic phase that begins to have a stable liquid phase at 469 ºC.

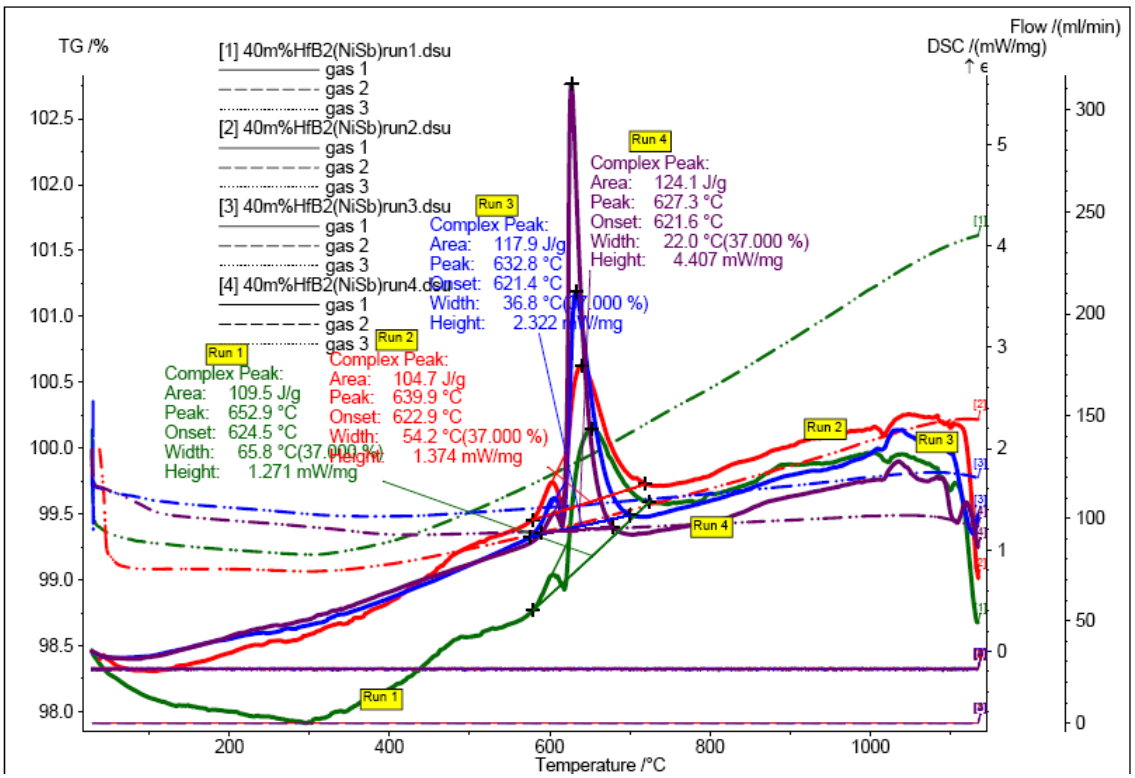

Figure 13: DSC curve for the nominal NiSb composition.

The Ni-Sb system exhibited DSC curves (Figure 13) of a similar shape to those in the Sb_2Hf (Figure 9); the curves are quite consistent from one trial to the next. However, the test runs using reduced nickel show the most clear parallel curves (Figure 14); the effect of using reduced nickel

is discussed in section 5.5. The exothermic reaction beginning around 600 ºC is soon interrupted by a small melting endotherm coinciding with the lowest temperature liquid from the Ni-Sb phase diagram of 616 ºC. The ignition temperature recorded in Table 6 is taken from the inflection point after this melting interruption due to the automatic software analysis described in section 4.3. Once again, there appear to be intermetallics forming in the solid-state just before melt formation.

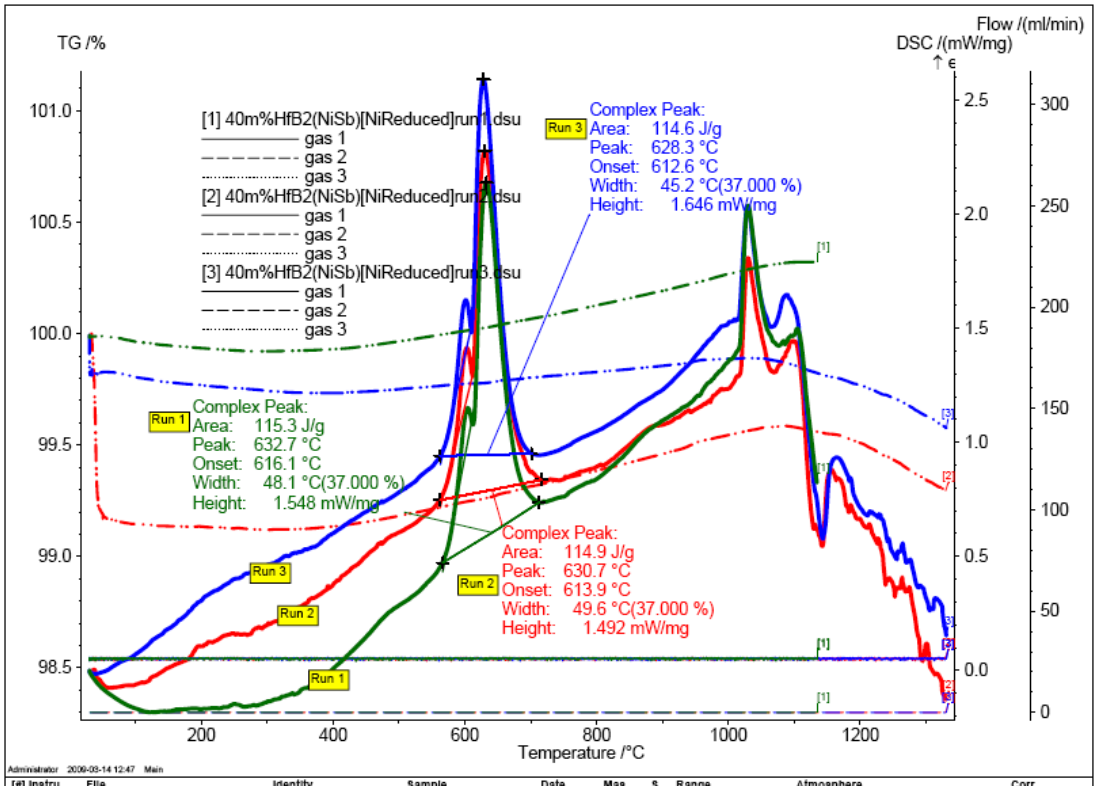

Figure 14: DSC curve for the nominal NiSb (Ni reduced) composition.

In summary, ignition temperatures correlate closely with lowest known temperatures at which stable liquids are found on binary phase diagrams, except in systems containing bismuth. An

artifact of the powder processing methodology is a large surface area present within the compacted blends. The interface between particles in a compact acts as a diffusion couple over which the entire range of phases present in a phase diagram may exist.

Figure 15 below depicts ignition temperatures as a function of the lowest melting temperature associated with a blend. The plotted line passes through the origin with a slope of one representing the case where ignition temperature equals the lowest melting temperature found throughout binary phase diagrams for a system.

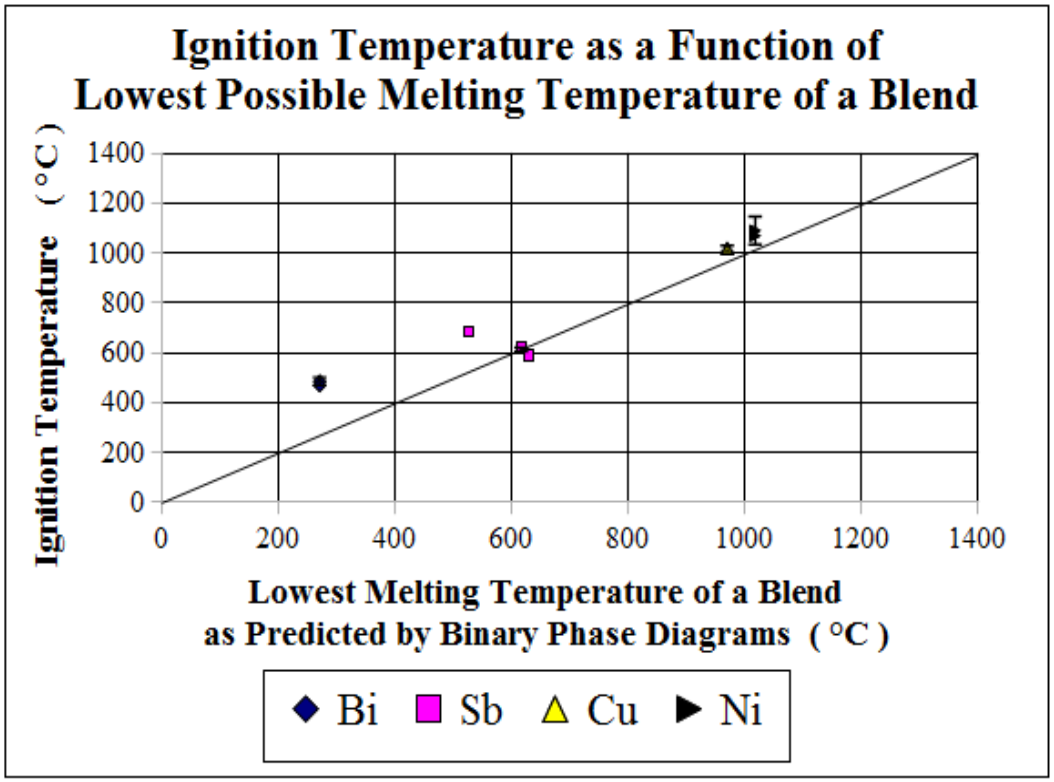

Figure 15: Ignition temperature as a function of the lowest possible melting temperature of a blend, predicted through consultation of binary phase diagrams.

Deviations from this line are seen at the lower extreme for compounds containing bismuth. Apparently there is a lower limiting temperature to initiate these reactions near 470 ºC, which may be accounted for by the melting of boron oxide or intermetallics formed during the heat cycle. The outlier in the group of systems containing antimony represents the Cu_2Sb blend. The DSC data for this composition shows two distinct endothermic and exothermic reactions as seen in Figure 11. The initial exothermic reaction occurs at a temperature very close to melt formation as predicted by the Cu-Sb binary phase diagram; however, ignition is recorded for the second, major exothermic event. The Cu_2Sb outlier is explained simply by the convention for recording reaction ignition temperatures.

5.2 Reaction Enthalpies

Table VII below summarizes the raw data interpreted for enthalpies of reaction from the DSC charts presented in the previous section (5.1). These data are less repeatable than ignition data, largely due to the fact these values are more affected by the shape of DSC results after integration over a temperature range. Standard deviations (σ) for several compositions are less than 10% of the mean; with the upper range of σ peaks around one quarter of the mean.

An interesting trend throughout nominal formulations is that the first trial tends to yield poorly defined reactions, such that accuracy may improve with subsequent trials; this is discussed in the summary of results, section 5.4. Below, each blend is addressed individually with reference made to the DSC curves presented in section 5.1 concerning ignition temperatures.

Table VII:
Reaction enthalpy experimental data from the DSC

Nominal Composition		Δ H (J/g)						
40 v%	60 v %	1	2	3	4	Average	StandardDeviation σ^a	Coefficient of Variance V^b
HfB_2	$Cu_{51}Hf_{14}$	---	238.6	333.8		286		
HfB_2	Ni_5Hf	---	74.5	90.5		82.5		
HfB_2	Ni_7Hf_2	304.6	179.2	290	300.1	268	59.84	0.22
HfB_2	NiHf	295	303.2	264.4	251.3	278	24.64	0.088
HfB_2	Sb_2Hf	---	70.9	113.7	114.6	100	24.97	0.25
HfB_2	Sn_2Hf							
HfB_2	Bi_2Hf	37.9	54.4	49.5	47.6	47.4	6.92	0.15
HfB_2	Cu_2Sb	---	131.5	128.5	---	130	2.12	0.016
HfB_2	NiBi	---	87.5	---		87.5		
HfB_2	NiSb	109.5	104.7	117.9	124.1	114	8.64	0.076
HfB_2	NiSb (NiReduced)	115.3	114.9	114.6		115	0.35	0.0031

a: Standard deviation omitted for two or less samples
b: Coefficient of variance simply means the standard deviation divided by the mean
--- indicates no clear reaction present for evaluation

For the $Cu_{51}Hf_{14}$ composition, DSC indicates a peak reaction enthalpy near 330 J/g (Figure 5). The maximum enthalpy, found during the final trial, is likely the most accurate because the first and second trials, respectively, show 25 % and 7 % mass gains. The mass gain appears to be associated with environmental contamination (see section 5.4) reacting with blend components and thereby hindering the formation of HfB_2. The larger enthalpy of the third trial indicates a more complete conversion of reactants into hafnium diboride. A small endothermic reaction is apparent around 1050-1080 ºC and likely corresponds to the melting of some residual Cu-Hf intermetallic.

The reaction enthalpies for matrices containing nickel-hafnium intermetallics are clearly seen to increase in size, clarity, and repeatability with decreasing amounts of nickel. This may indicate that formulations rich in nickel tended to form intermetallics, hindering peak reaction enthalpies. Exothermic reaction enthalpies were on the order of 80 J/g for the Ni_5Hf composition (Figure 6), and 300 J/g for the Ni_7Hf_2 (Figure 7) and NiHf systems (Figure 8). The NiHf composition had the smallest standard deviation for nickel blends; it showed a decrease in enthalpy for the final two trials, measuring approximately 250 J/g. Although unclear, this may be an artifact of time delay and atmospheric exposure, interference from intermetallics, or simply normal data scatter.

The reaction enthalpy for the Sb_2Hf system (Figure 9) is approximately 115 J/g. As discussed in the previous section, the exotherm is interrupted by a melting endotherm; possibly indicative of intermetallic formation. The low reaction enthalpy supports this conjecture; intermetallics formed during this reaction may serve to limit the formation of HfB_2 as the final product, thereby limiting energy released.

The reaction enthalpy for the Bi_2Hf composition (Figure 10) showed maximum exothermic peaks of about 50 J/g. No further endotherms indicate any melting; although the signal shows fluctuations above 800ºC, there are no distinct reactions. Similarly, the DSC curves for NiBi (Figure 12) exhibit variation in magnitude of exothermic reactions stemming from different curve shapes; the maximum enthalpy measured was near 87 J/g. For the NiBi blend, unclear fluctuations are prevalent in the DSC signal and increase above 1000 ºC. The low reaction enthalpies for these bismuth containing compositions support the possibility of intermetallic formation.

The largest exothermic peaks for the Cu_2Sb system (Figure 11) begin around 685ºC and are approximately 130 J/g in magnitude. For this system the formation of intermetallics is particularly clear from the two distinct pairs of endo/exothermic reactions. Once again, reaction enthalpy appears to be limited by the formation of intermetallics.

The shape of the DSC curves for the NiSb system (Figure 13) is similar to that of the Sb_2Hf system (Figure 9), especially for the formulation using reduced nickel (Figure 14). The reaction enthalpies are approximately 115 J/g and support the theory of intermetallic formation limiting reaction completion. Further, the curves produced from the reduced nickel composition indicate additional reactions happening between 1050 ºC and 1150ºC. These reactions may indicate the deterioration and melting of Ni-Sb intermetallics, which the Ni-Sb phase diagram indicates may be stable in solid form up to 1161 ºC.

5.3 Maximum Reaction Temperatures

The pyrometry data, shown in Table VIII, generally showed large variations. However, given inherent limitations of the instrument as discussed in section 3.2, deviations of over 60 ºC are expected for an ideal blackbody measurement. Although our samples are certainly not perfect blackbodies, metals and inter-metallics tend to have high emissivities. A mixture of HfB_2 + 5 w% $MoSi_2$, a sintering additive, has been reported to have an emissivity of 0.9 (2). Evaluation of standard deviations is omitted due to the limited number or trials; known variations of monitoring equipment exceed these values in several cases.

Table VIII:
Maximum temperatures of reaction measured by two-color pyrometry

Nominal Composition		T max (°C)		
40 v%	60 v %	1	2	Average
HfB_2	$Cu_{51}Hf_{14}$ *	2237	2163	2200
HfB_2	Ni_5Hf	2106	2089	2097.5
HfB_2	Ni_7Hf_2	2063	2215	2139
HfB_2	NiHf *	2345	---	
HfB_2	Sb_2Hf *	---	2397	
HfB_2	Sn_2Hf *	2860	2230	2545
HfB_2	Bi_2Hf +	2018	1849	1933.5
HfB_2	Cu_2Sb +	1963	1867	1915
HfB_2	NiBi +	1746	1585	1665.5
HfB_2	NiSb +	1867	1850	1858.5
HfB_2	NiSb + (NiReduced)	1909	1986	1947.5

* Max temperatures coincided with first temperature measured for these blends
+ The temperature profiles for these compositions clearly indicate intermediate formation by the presence of multiple maxima

For some trials, the maximum registered temperature is recorded with the first data point; in these cases, noted above in Table VIII, higher temperatures are possible prior to instrument response time. Additionally, the shape of some temperature curves exhibit several local maxima, usually two, further supporting of the formation of intermediate compounds; these are also noted above. Table VIII only reflects the largest temperature recorded.

The Ni_5Hf pyrometry data confirms the ignition temperature to be near 1050 ºC. However, the other nickel-hafnium blends do not indicate ignition by pyrometry. Several compositions appear to ignite above 1000 ºC prior to max temperature attainment including: Cu_2Sb, Bi_2Hf, NiBi, and NiSb. This evidence suggests further reactions taking place that are not measured through the

DSC and may be responsible for the maximum temperature. The Sb_2Hf and Sn_2Hf compositions are observed to dissociate as the pellet reacts, making it difficult to accurately measure the temperature. With only a specific area targeted by the pyrometer, things happening outside the scope only register by reflected radiation which loses intensity as it travels.

Notably, the box furnace is exposed to the atmosphere allowing further complications of reaction dynamics. For example, experiments indicate significant reactions exist between pure titanium and gaseous nitrogen (8); oxidation of the raw materials is also widely known to accelerate with increasing temperatures. Environmental interactions may well affect measurements of peak reaction temperatures.

5.4 Powder X-Ray Diffraction

For all compositions, XRD data depicts strong diffraction peaks revealing the presence of HfB_2 as seen in Figures 16-22. In one case, Cu_2Sb, diffraction peaks clearly indicate formation of intermetallics, highlighted in Figure 21. The NiSb diffraction pattern also indicates the formation of an intermetallic structure, though the NiSb peaks of Figure 22 are all shifted to the right. Ni_5Hf and Ni_7Hf_2 both exhibited unidentified peaks that may be due to the formation of a poorly characterized phase or amorphous structure.

A minute quantity of hafnium oxide is detectable in many compositions, including: Ni_5Hf, Ni_7Hf_2, Sb_2Hf, Cu_2Sb, and NiSb. XRD intensity peaks for both nickel-hafnium formulations (Ni_5Hf, Ni_7Hf_2) indicate small amounts of hafnium nitride present in the final product (see

Figures 17 and 18). No diffraction experiments were conducted for the NiHf, Sn_2Hf, and NiBi systems due to inadequate quantities of material available following reaction in the box furnace.

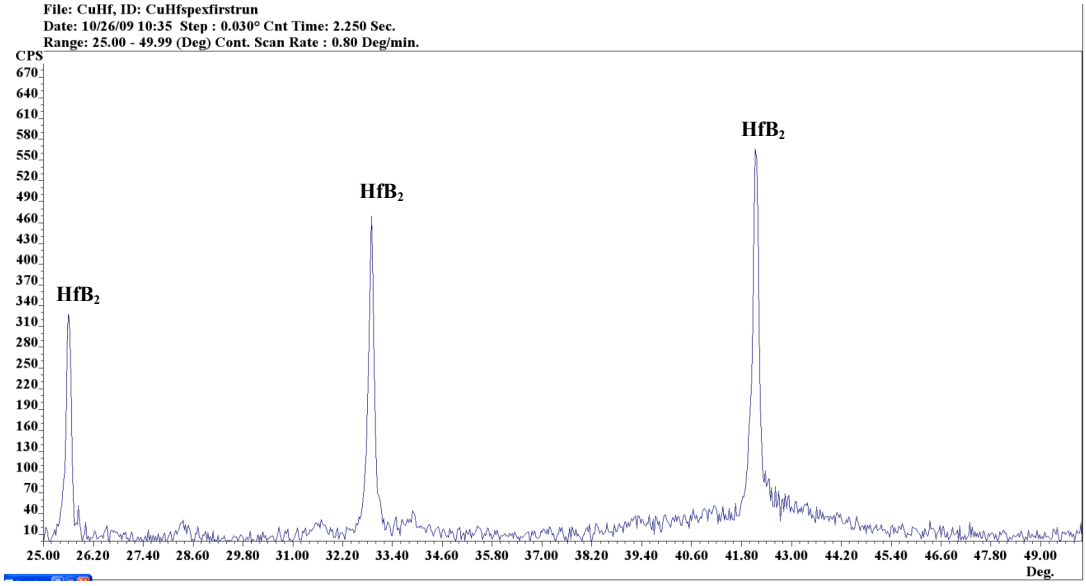

Figure 16: XRD results for the nominal $Cu_{51}Hf_{14}$ composition.

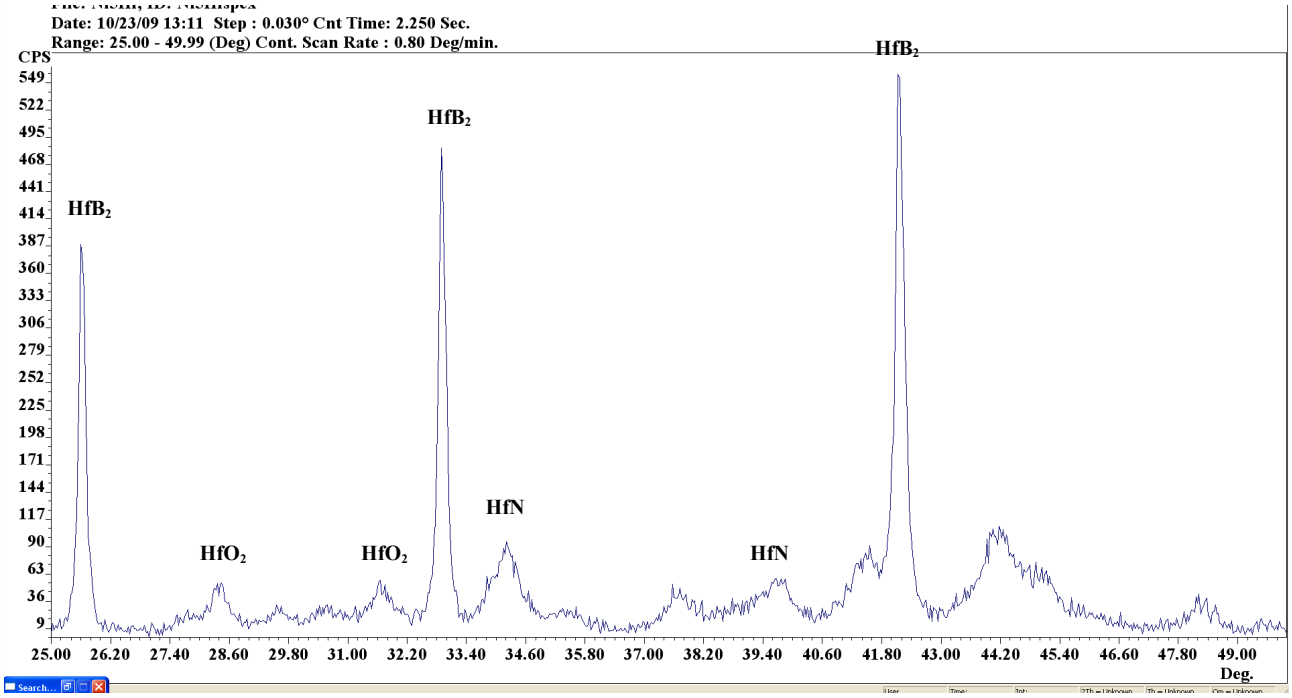

Figure 17: XRD results for the nominal Ni_5Hf composition.

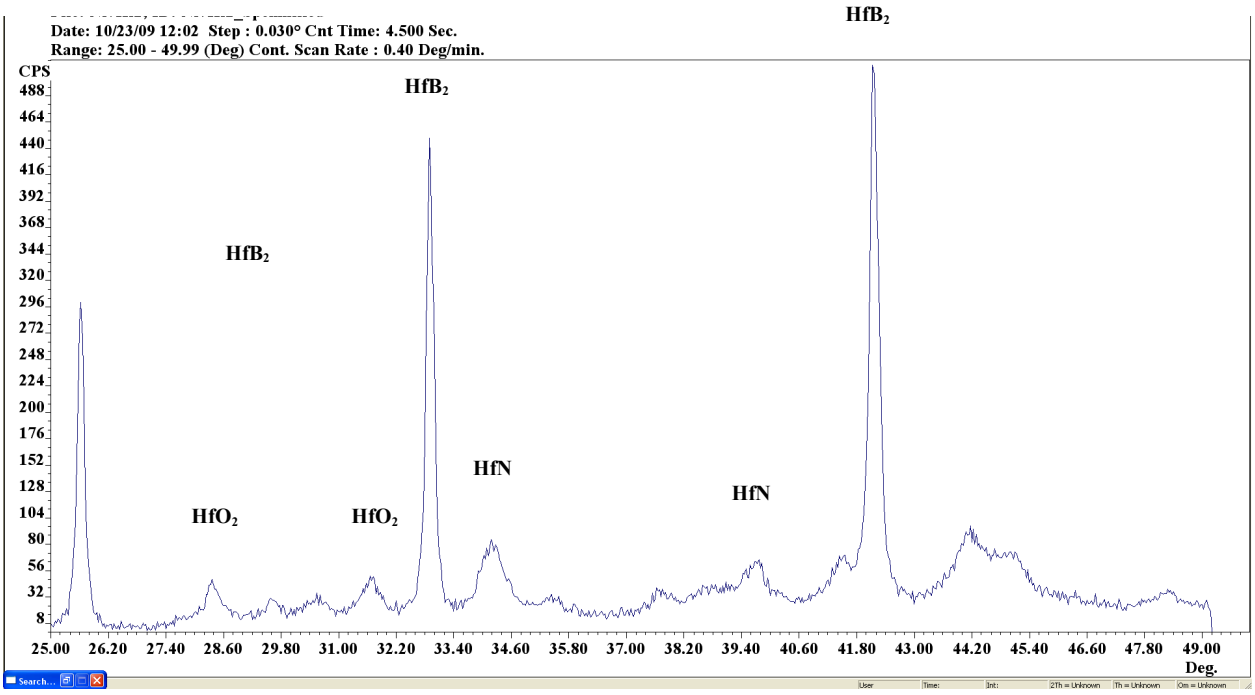

Figure 18: XRD results for nominal Ni_7Hf_2 composition.

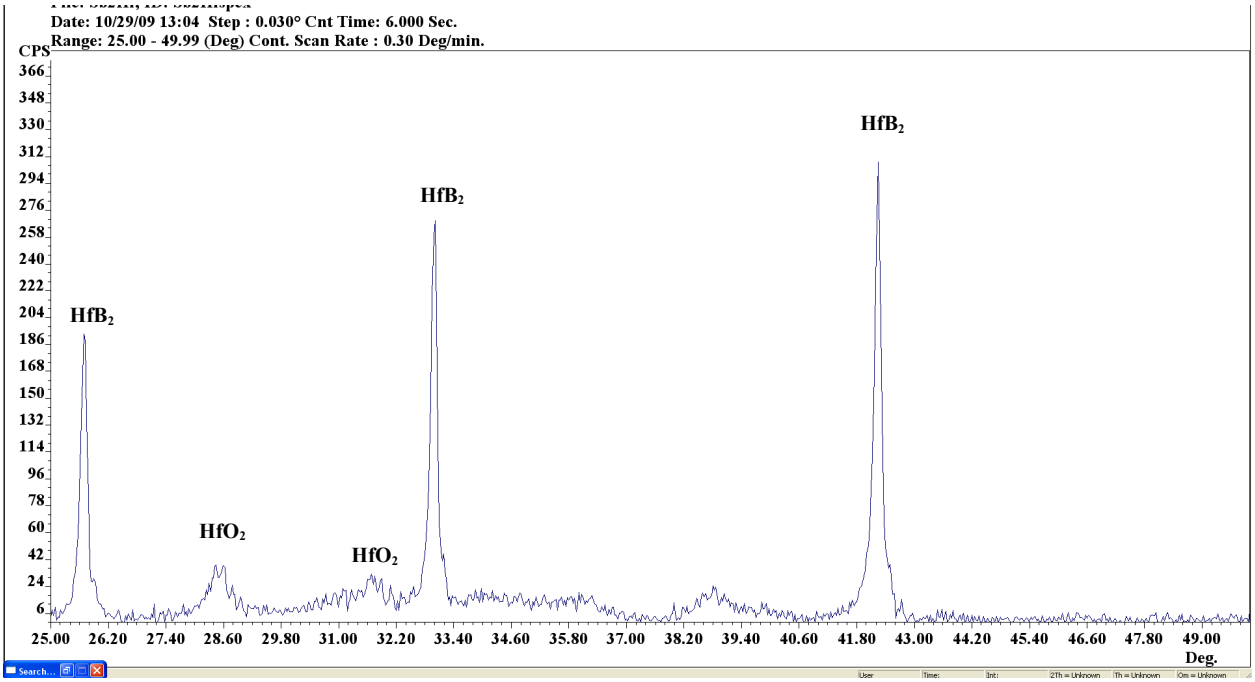

Figure 19: XRD results for nominal Sb_2Hf composition.

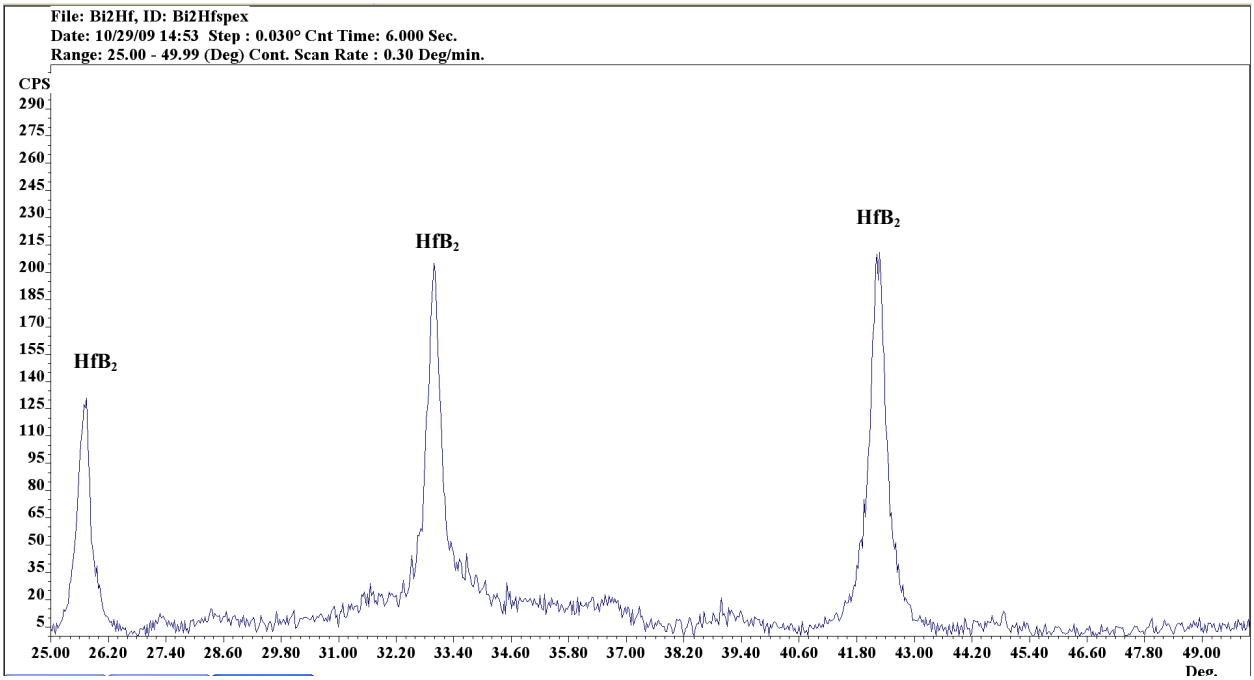

Figure 20: XRD results for the nominal Bi_2Hf composition.

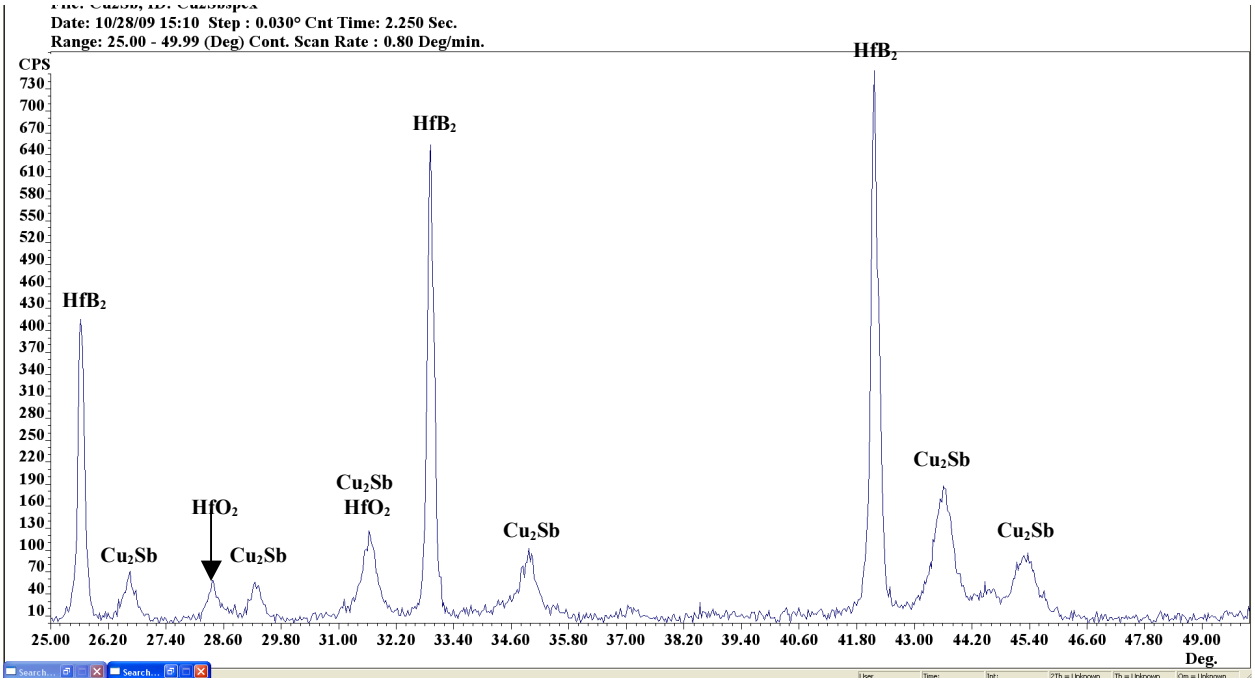

Figure 21: XRD results for the nominal Cu_2Sb composition.

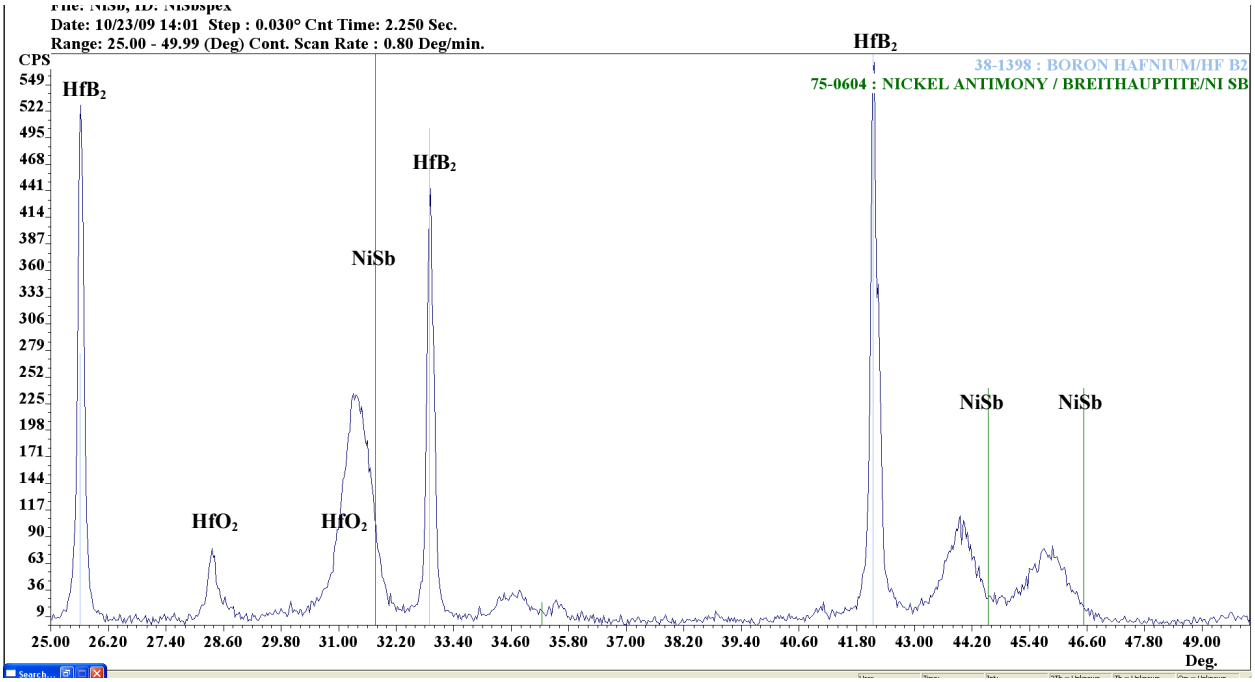

Figure 22: XRD results for the nominal NiSb composition.

5.5 Discussion of Sb, Bi, Cu, Ni, Sn blends

Below, certain particulars about the blends are discussed. One section is devoted to each ductile matrix and will address trends throughout formulated compositions which include that element. DSC curves are presented in section 5.1.

Antimony

Matrix formulations containing antimony include Sb_2Hf, Cu_2Sb, and NiSb. Pure antimony is observed to melt around 630 ºC at atmospheric conditions and boil at 1750 ºC. The Sb_2Hf and NiSb compositions are found to ignite below the melting of pure antimony by 30-50 ºC as seen in Table VI. All maximum temperatures recorded through pyrometry exceed the boiling temperature of antimony as seen in Table VIII. However the DSC results did not show a subsequent loss in mass, suggesting that intermetallics formed in a zone around the region of peak combustion temperatures.

No phase diagram is available for the Hf-Sb system. Phase diagrams for the Ti-Sb and Zr-Sb systems are available, though made from sparse data, as implied by the dotted lines. However, they do serve to indicate the presence of stable intermediate compounds; hafnium tends to exhibit similar properties with titanium and zirconium, therefore, it also is likely to have some stable phases with antimony.

Bismuth

Compositions formulated with bismuth include Bi_2Hf and NiBi; bismuth is known to melt in its pure form around 270 ºC and boil near 1560 ºC. Once again the measured maximum temperatures exceed the boiling temperature of pure bismuth; only the NiBi blend exhibited a

mass loss beginning near 1200 ºC on the DSC curve, shown in Figure 12. DSC curves for both bismuth compositions showed melting near 270 ºC followed by an exothermic reaction around 470 ºC; subsequent heating results in various poorly defined reactions. There appears to be a lower limit for ignition temperatures with DSC heating rates (40 ºC/min) found for both bismuth blends.

Copper

Phases with copper include $Cu_{51}Hf_{14}$ and Cu_2Sb; copper melts around 1080 ºC. The DSC curves show a significant mass increase of approximately 25 % that accompanies the first trial. The second trial appears to gain about 7 % in mass. This system has the most noticeable increase in mass, likely caused by contamination as previously explained in section 5.5 above.

Nickel

Formulations containing nickel include Ni_5Hf, Ni_7Hf_2, NiHf, NiBi, and NiSb. The three compositions with hafnium allow for an investigation into compositional effects and are found to ignite well below the melting temperature of pure nickel. The DSC reactions are fairly consistent and increase in uniformity with compositions richer in hafnium; or in other words, the NiHf trials are very consistent, while the Ni_7Hf_2 and Ni_5Hf blends are increasingly variable.

These compositions ignited around 1100 ºC, following a very small endothermic reaction that appeared to decrease in size with decreasing nickel content. The Ni_5Hf formulation displayed a much smaller exothermic reaction than the other two systems. The Ni_5Hf and Ni_7Hf_2 blends also show an endotherm near 1200 ºC. The final melting endotherms could be accounted for by the melting of one of the numerous intermediary compounds between nickel and hafnium.

The Ni-Sb system is repeated with reduced nickel powders that have first been subjected to heating in an H_2 atmosphere to reduce surface oxidation. Although the reactions appear to begin at nearly the same temperature, the shape of the DSC curve elongates vertically for the reduced nickel. The elongation implies a quicker reaction and may be an artifact of remnant hydrogen, present in the form of nickel hydrides. These hydrides may reduce nearby oxides or carbonaceous material introduced through lubricants driving the reaction to completion more quickly once initiated. Although both data sets are very consistent, the DSC curves for reduced trials form three almost completely parallel curves indicating that remnant oxide of the raw materials affects experimental repeatability. The DSC curve shows additional reactions between 1050ºC and 1150 ºC. This final endotherm at 1150ºC matches with the melting temperature of the NiSb phase.

Tin

The tin system investigated yielded no clear reactions. Upon examining the sample remainder following the DSC trials, it became apparent that the tin melts and separates from the rest of the blend. A film of tin on top of a crumbly mixture, which clearly contains boron, is found in samples subjected to DSC runs that indicate no clear reaction. However, empirical observation of this composition reacted in a box furnace clearly supports an energetic reaction. The discrepancy between the DSC and box furnace heating rates certainly explains this anomaly. However, the bismuth compositions yielded reactions in the DSC despite their low melting temperatures. The maximum temperatures recorded for this composition are especially questionable; during reaction in the box furnace, this compact is observed to dissociate, or come apart, making an accurate temperature measurement challenging.

5.6 Summary of Results

The collection of ignition temperatures determined through DSC yielded consistent data both within a dataset, and for varying compositions. This suggests that ignition may depend on a single event. Generally, ignition is preceded by a melting endotherm that corresponds with melt formation at temperatures indicated on binary phase diagrams as discussed in section 5.1.

Some formulations lack a melting endotherm prior to the exothermic reaction, which may indicate the formation of intermetallics directly from a solid phase; this was observed for Sb_2Hf, NiSb, and $Cu_{51}Hf_{14}$ systems. However, examination of phase diagrams indicates the presence of stable liquid at temperatures below the exothermic reactions for the $Cu_{51}Hf_{14}$ composition. The Sb-Hf, and Sb-B phase diagrams are not available for examination.

Throughout blends, a common trend in DSC data may explain a repetitive source of variation. Numerous compositions exhibited an increase in mass during the initial trial, which subsequently dropped in later trials. In fact, an incremental decrease in mass gain with progressive trials is seen in the following systems with the approximate peak mass gains for the initial and subsequent trials in parentheses: $Cu_{51}Hf_{14}$ (25% → 7% → 2%), Sb_2Hf(12% → 5% → <1%), NiBi(6% → 7% → 1%), seen in Figures 5, 9,and 12, respectively.

The DSC is shared by numerous researchers; some experiments that investigate curing may leave behind organic residues on the internal DSC chamber surface from evaporated binding agents.

These residues are likely the cause of mass gain during initial trials, which effectively clean the chamber for subsequent runs. Interpretation of ignition temperatures for initial trials is largely unaffected by these contamination effects. Ignition of a poorly defined reaction for the first trial is observed to coincide with clear reactions found in subsequent trials; except in the $Cu_{51}Hf_{14}$. The environmental interaction is likely to reduce measured enthalpies due to the consumption of elemental components, which thereby reduces precursors available to form HfB_2.

The reaction enthalpies are most useful in a qualitative manner for confirmation rather than quantitative comparison. Enthalpies reveal that many of the exothermic reactions appear to be limited by the formation of intermetallics. Only the $Cu_{51}Hf_{14}$, Ni_7Hf_2, and NiHf compositions attained maximal exothermic output near 300 J/g. However, the maximum temperatures measured through pryometry show Ni_5Hf and Sb_2Hf compositions with similar reaction temperatures to the formulations with 300 J/g exotherms. Additionally, pyrometry data indicates numerous reaction ignitions above 1000 ºC as discussed in section 5.3. These inconsistencies may stem from the disparity of heating rates between the two measurement techniques or may suggest inherent errors in pyrometry.

X-ray diffraction analysis confirms the presence of HfB_2 in the post-reacted products for all formulations examined. In at least one case, Cu_2Sb, diffraction data clearly indicates the existence of a crystalline intermetallic.

Conclusions

The supposition that the formation of melt precedes and drives the main exothermic reaction is mostly true. Further, consultation of several binary phase diagrams seems to be sufficient in approximating the temperature of melt formation. For the lower extreme, there appears to be a threshold temperature that must be exceeded to initiate combustion.

The reaction sequence seems to include the formation of intermetallics in most cases. The Cu-Sb system clearly depicts intermetallic formation confirmed through XRD. Ni-Hf systems exhibit reactions after the primary exotherm, which indicate activity of the intermetallics formed. Sb-Hf and Ni-Sb compositions begin with an exothermic reaction, which appears to be interrupted by an endotherm. These interruptions may represent the formation of solid intermediate compounds at the beginning of the reaction sequence, which subsequently melt.

The DSC results can be improved by beginning each new sample series with a cleaning run to minimize residues and obtain more repeatable reaction enthalpies. Environmental contamination and instrumental lag could be further marginalized by reacting larger samples in a higher capacity calorimeter.

The peak temperature measurements appear to have little correlation with the corresponding enthalpies of reaction and may simply indicate that pyrometry is not a sufficient temperature measurement technique. However, there is also evidence to suggest that the energetic events measured through pyrometry do not coincide with those measured through DSC. The lack of a

parallel between these results underscores the need for a method to compare ignition, enthalpy, and peak temperature with a single continuous system, with a common heating rate and controlled atmosphere.

Future Work

A natural extension of this project would seek to rectify the different heating rates of the DSC and box furnace. One way to do this could utilize a large capacity calorimeter and measure the peak temperatures concurrently. However, the discrepancies may simply be an artifact of the inherently large errors associated with two-color pyrometry. Study of the reaction front to determine exactly where the maximum spectral radiance comes from and careful study of the emissivity of the phases radiating peak temperatures may allow for a single color pyrometer to yield more accurate data.

Future experimentation with the DSC may be improved by beginning each set of trials with a cleaning run in which the DSC chamber is heated up with a generous supply of air to ensure interaction with residues is limited during subsequent trials.

Further exploring the bismuth systems could confirm lower reaction limits. An initial examination of metals with melting temperatures below 450 ºC may give insight to the boron oxide postulate. A high heating rate calorimeter used to reexamine the tin system may also allow for ignition temperature measurement. Introduction of a reducing agent into these systems may also help examine this lower boundary temperature.

Investigating the peak temperatures of samples reacted in a furnace with a controlled argon atmosphere may help to rectify inherent environmental affects with DSC data. A shielded reaction chamber could also allow the concurrent use of a thermocouple for reactions with peak temperatures within thermocouple limits.

References

1. **Yi, H.C. Woodger, T.C. Moore, J.J. Guigné J.Y.** Combustion Synthesis of HfB_2-Al Composites. *Metallurgical and Materials Transactions B*. Volume 29B (August 1998). p. 877-887

2. **Savino, R. Fumo, M.D.S. Silvestroni, L. Sciti, D.** Arc-jet testing on HfB_2 and HfC-based ultra-high temperature ceramic materials. *J. Am. Ceram. Soc.* 28 (2008) 1899-1907.

3. **CES: Cambridge Engineering Selector.** Granta Design Limited, *software version 4.6.1.* 2006.

4. **Passerone, A. Muolo, M.L. Valenza, F. Monteverde, F. Sobczak, N.** Wetting and Interfacial Phenomenon in Ni-HfB_2 systems. *Acta Materialia 57* (2009) 356-364.

5. **Gasch, M. Johnson, S.** Thermal Conductivity Characterization of Hafnium Diboride-Based Ultra-High-Temperature Ceramics. *J. Am. Ceram. Soc. 91* (2008) 1423-1432.

6. **Chemix**, evaluation copy. Arne Standnes. Educational chemistry *software version 3.50.* 2009

7. **Weimer, Alan;** Editor. Carbide, Nitride, and Boride Materials Synthesis and Processing. Chapman and Hall. 1997.

8. **Merzhanov, A. G.** Reviews: Fundamentals, achievements, and perspectives for development of solid-flame combustion. *Russian Chemical Bulletin Vol. 46 No.1* (January 1997)

9. **Glassman, Irvin.** Combustion. Third Edition. *Academic Press.* 1996. p. 451-462

10. **Ma, Z.Y. Tjong, S.C.** *In Situ* Ceramic Particle-Reinforced Aluminum Matrix Composites Fabricated by Reaction Pressing in the TiO_2 (Ti)-Al-B (B_2O_3) Systems. *Metallurgical and Materials Transactions A. Volume 28A* (September 1997). p. 1931-1942.

11. **Hull, D.** Introduction to dislocations. 2nd Ed. *Pergamon Press.* 1975. p. 15-28, 192-215

12. **German, Randall M.** Sintering Theory and Practice. *John Wiley & Sons.* 1996. p. 1-15, 225-247, 395-402

13. **Philibert, Jean.** Atom Movements: Diffusion and Mass Transport in Solids. Translated by: Steven J. Rothman. *Les Éditions de Physiques 1991.* p. 1-18, 251-270, 425

14. **Gartenberg, E.** Infrared Thermography. Temperature Measurements. April 22-26, 1996. *von Karmen Institute for Fluid Dynamics: Lecture Series 1996-07.*

15. **Gülhan, A.** Introduction to pyrometry and comparison of different pyrometer configurations. Temperature Measurements. April 22-26, 1996. *von Karmen Institute for Fluid Dynamics: Lecture Series 1996-07.*

16. **LumaSense Technologies Inc.** TN-833: Understanding Two-Color (Ratio) Pyrometer Accuracy. Figure 3. Available by request from: LumaSense Technologies at www.lumasenseinc.com

Appendix A: Additional DSC Curve

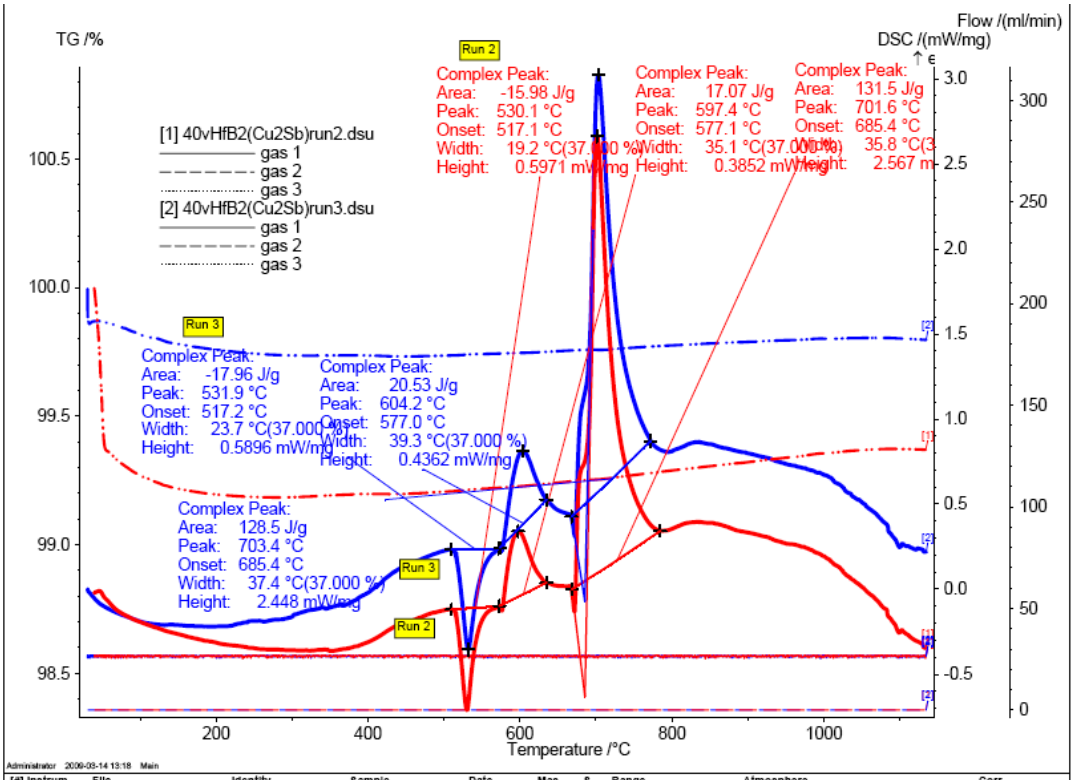

A1: DSC curve for the nominal Cu_2Sb composition (enlargement of trials 2 and 3)